



This is a repository copy of *Critical insights into real-time granule size characterisation during segmented fluid-bed drying as part of a continuous ConsiGma™25 system*.

White Rose Research Online URL for this paper:

<https://eprints.whiterose.ac.uk/id/eprint/229487/>

Version: Accepted Version

---

**Article:**

Bungău, J.-M. and Salman, A.D. [orcid.org/0000-0001-6766-7254](https://orcid.org/0000-0001-6766-7254) (2025) Critical insights into real-time granule size characterisation during segmented fluid-bed drying as part of a continuous ConsiGma™25 system. *Powder Technology*, 464. 121197. ISSN 0032-5910

<https://doi.org/10.1016/j.powtec.2025.121197>

---

© 2025 The Authors. Except as otherwise noted, this author-accepted version of a journal article published in *Powder Technology* is made available via the University of Sheffield Research Publications and Copyright Policy under the terms of the Creative Commons Attribution 4.0 International License (CC-BY 4.0), which permits unrestricted use, distribution and reproduction in any medium, provided the original work is properly cited. To view a copy of this licence, visit <http://creativecommons.org/licenses/by/4.0/>

**Reuse**

This article is distributed under the terms of the Creative Commons Attribution (CC BY) licence. This licence allows you to distribute, remix, tweak, and build upon the work, even commercially, as long as you credit the authors for the original work. More information and the full terms of the licence here: <https://creativecommons.org/licenses/>

**Takedown**

If you consider content in White Rose Research Online to be in breach of UK law, please notify us by emailing [eprints@whiterose.ac.uk](mailto:eprints@whiterose.ac.uk) including the URL of the record and the reason for the withdrawal request.



[eprints@whiterose.ac.uk](mailto:eprints@whiterose.ac.uk)  
<https://eprints.whiterose.ac.uk/>

# CRITICAL INSIGHTS INTO REAL-TIME GRANULE SIZE CHARACTERISATION DURING SEGMENTED FLUID-BED DRYING AS PART OF A CONTINUOUS CONSIGMA™25 SYSTEM

Jeanina-Monica Bungău & Agba D. Salman

School of Chemical, Materials and Biological Engineering, The University of Sheffield, UK

E-mail: [jmbungau1@sheffield.ac.uk](mailto:jmbungau1@sheffield.ac.uk)

## ABSTRACT

This study demonstrates the implementation of a Parsum IPP70-S real-time granule size monitoring system within the segmented fluid-bed dryer of the ConsiGma™25 continuous manufacturing line. Reference real-time patterns were established for granules produced at liquid-to-solid (L/S) ratios of 0.15, 0.3 and 0.4, developing a comprehensive understanding of granule size throughout the entire drying process. The in-line measurements were found to be influenced not only by the size of individual granules passing through probe's optics, but also by granules' movement as a population during the process. It was also highlighted that the filling phase causes erratic granule movement, which further affects the real-time characterisation. Increasing the L/S ratio resulted in the formation of larger granules and a significant reduction in granule detection rate – from a maximum of 2500 granules/s at L/S 0.15 to 270 granules/s at L/S 0.4 – while the moisture content post-drying ranged from 2.4% to 10.8%. Granules formed under the highest L/S ratio also imposed processing and measurement limitations due to extensive liquid bridge formation, ultimately leading to channelling. Furthermore, off-line validation confirmed that overlapping granules distort Parsum size estimations, particularly causing overestimations of the Dv90 percentile by up to 13.97%. Lastly, to support real-time decision making and ensure compliance with regulatory guidelines for continuous manufacturing regarding determination of any irregularities during processing, intentional process disturbances were created. By varying the L/S ratio from 0.15 to 0.4 during operation, size deviations from reference trends were detected and characterised in-line, enabling early detection of process deviations using sensory measurement techniques.

## KEYWORDS

Real-time granule size analysis; Continuous wet granulation; Segmented fluid-bed drying; Process disturbance

## 1. INTRODUCTION

Pharmaceutical tablets are currently the most prevalently used medicines, addressing the critical importance of precise product development and subsequent manufacturing at industrial scales. Continuous pharmaceutical manufacturing (CPM) is perceived as a versatile, robust and advantageous incentive which implies end-to-end production, with all the unit operations interconnected in series [1]. Some of the benefits associated to CPM refer to enhanced raw materials and product critical quality attributes (CQAs), speed to market, improved sustainability, reduced spatial requirements and material and energy waste [2,3].

Quality control is one of the governing factors within the pharmaceutical sector and, in terms of quality assurance at industrial scales it has been mostly dependent on statistical process control and off-line characterisation methods. Achieving complete process control within continuous lines can be challenging due to system's inherent complexity, performance uncertainties, various process and

formulation parameters to be considered and especially in-process quality control. These issues further result in industrial reluctance regarding widespread applicability and adoption of advanced process control strategies, which strongly suggests that the pharmaceutical sector, and more specifically the continuous manufacturing area still requires appropriate understanding of certain complex matters [4]. More importantly, the International Council for Harmonisation (ICH) has recently released the Q13 guidance for industry implementation on “Continuous Manufacturing of Drug Substances and Drug Products” [5]. The guidance clearly states that control strategies alongside achieving state of control in CPM is of critical importance for successful production of continuously manufactured solid forms [5]. Additionally, it is emphasised that any source of disturbance and drift from an expected trend must be identified through frequent process monitoring.

In order to facilitate the flexibility of a well-known continuous system – the ConsiGma™25 line – which commonly operates with minimal real-time CQAs monitoring and pre-determined process parameters [6], more attention must be paid to granules’ characteristics and behaviour in real-time. Nonetheless, determining the effect of process variations or sudden disturbances on intermediate products’ characteristics should be of high priority. Hence, implementation of in-line process analytical technologies (PAT), capable of providing real-time information with regards to the CQAs of interest during processing in some of the most significant unit operations can address and resolve any uncertainties referring to system performance, intermediate product deviations and its effect on the final product and ultimately allow real-time decision making when necessary.

One of the most important unit operations integrated within the ConsiGma™25 powder-to-tablet line is the segmented fluid-bed dryer (FBD). It has been established that the dryer has the most substantial impact on granules’ residence time, as well as being the highest energy-consuming equipment [7,8]. Furthermore, the studied impact of various dryer associated process parameters demonstrate the essential role it plays in achieving qualitative granule characteristics. When referring to intermediate products in pharmaceutical manufacturing one of the most fundamental critical quality attributes (CQA) is the granule size distribution (GSD). Granule size variability can significantly impact the quality of the final product to such extent that segregation, inefficient dissolution profiles, tablet aspect or internal structure irregularities could occur [9]. Although many parameters can influence granules’ CQAs [10,11], it is known that liquid to solid ratio (L/S ratio) is the most significant [12–15]. In terms of the effect of varying the L/S ratio on granules’ GSD the general trend expressed that using low L/S ratios during twin-screw granulation, high fraction of fines are produced, whereas increasing this parameter leads to the formation of larger fraction containing coarse granules being formed [7,13,14,16,17].

The need for improvement and time efficiency in terms of both production and granule characterisation has led to the development of more rapid and accurate sizing equipment. Depending on the application, several on-line and in-line methods exist [18,19]. Spatial filter velocimetry (SFV) is a sensory granule measurement technique based on evaluating shadow images of moving particles. This sizing principle implies determination of an individual granule’s characteristics passing through an optical fibre field of measurement (or laser beam channel), by measuring the chord length of granule’s projected area [19]. A thorough description of the SFV measuring principle has been offered in a previous study [20]. Although, the application of SFV for GSD measurements has been extensively investigated throughout the years, a vast majority of the published work focus on either fluid-bed granulation [21–23], high-shear mixing [20], coating [24,25] or roller-compaction [26,27]. In terms of SFV application for twin-screw continuous manufacturing, the reported literature is currently limited. A recent paper used a Parsum IPP-70 probe for off-line validation of granules’ median volumetric percentile (Dv50) [28], whereas only a few studies used SFV for real-time investigation of wet granules produced using a ConsiGma™25 system [6,29,30]. While these papers highlighted the applicability of the Parsum probe for real-time measurement of agglomerates produced by twin-screw granulation, their main focus was solely on the measurement of wet granules.

The in-line integration of a Parsum probe within other critical subsequent unit operations interconnected within the ConsiGma™25 line, such as the FBD, and the possible impact on real-time granule size measurement and behaviour was not considered. This aspect is of particular importance considering that the dryer is a highly influential equipment due to its significant effect on granule's CQAs and residence time.

Accurate granule size determination is of critical importance when performing in-process real-time investigation. While sensory measurement techniques offer numerous advantages, it is also important to consider the reported drawbacks, with fouling being a reoccurring issue during in-line measurements [19,30,31]. Additionally, coincidence instances – where two or more granules pass through probe's field of measurement at the same time (overlapping) and being inaccurately measured as a single large granule – are known disadvantages imposed by sensory probes. An earlier study [19] investigated this using an SFV probe with perfectly spherical particles (pellets and granules), exclusively through off-line methods.

### **1.1. Objectives**

The current paper aimed to conduct a preliminary investigation into how overlapping of elongated granules (i.e., coincidence instances) – produced via twin-screw granulation – affects size representation during real-time measurements using SFV. Granules produced with the ConsiGma™25 were subjected to benchtop experiments using a Parsum IPP70-S probe, during which feeding was performed at two different feed rates to assess the impact of throughput on measurement accuracy by comparing granules' percentiles. This factor holds significant relevance, as depending on granules' orientation when passing through the measurement field, elongated granules could lead to the detection of wider range of apparent sizes, alternatively being impacted by coincidence instances.

Moreover, the main focus of the present study imposed using a Parsum IPP70-S probe in-line, being placed inside the ConsiGma™25 integrated vertical six-segmented FBD. The L/S ratio was chosen as a primary CPP of focus, as being one of the most important CPPs in wet granulation, its variation will definitely impact the granule size. Three various L/S ratios were investigated, and a reference real-time granule behaviour based on the granule size and granule rate achieved during drying, as well as their final moisture content was determined. Any systematic factors being the cause of high fluctuations with time were also critically evaluated.

Further experimental work looked at purposely creating irregularities within the system with a final aim of understanding how significantly different granules behave as a population during the entirety of the drying process. The evaluation and data achieved through alterations in the most important CPP and its impact on granules' CQAs, and nonetheless the operational influence on granules' real-time behaviour during fluid-bed drying could serve as a reference for improving system's flexibility and hence optimise the CPM process. If deviations from the presently provided trends occur, it is recommended that thorough investigation is performed as these could suggest process instabilities that might affect the product. Furthermore, the current real-time SFV approach could be potentially adopted as a new effective implementation methodology for in-line GSD measurement and granule behaviour observation. This is based on the fact that no other studies are known to have previously reported the incorporation of a Parsum probe during fluid-bed drying as part of a continuous system [8,31].

## 2. MATERIALS AND METHODS

### 2.1. Materials

The raw materials used were  $\alpha$ -lactose monohydrate 200M (Volac International Ltd., Orwell, Royston, Herts, UK), microcrystalline cellulose (MCC) Avicel PH101 (Chemfield Cellulose Pvt. Ltd., Nagpur, Maharashtra, India) and low-substituted hydroxypropyl cellulose (HPC) LH-21 (Shin-Etsu Chemical Co. Ltd., Chiyoda-ku, Tokyo, Japan). All materials were pharmaceutical grade, with purities of 99.5% for  $\alpha$ -lactose monohydrate, > 93% for MCC and  $\geq$  94% for HPC. Particle sizes (Dv10, Dv50, Dv90) were 11  $\mu$ m, 54  $\mu$ m, 174  $\mu$ m for lactose; 18  $\mu$ m, 46  $\mu$ m, 99  $\mu$ m for MCC; and 18  $\mu$ m, 41  $\mu$ m, 67  $\mu$ m for HPC. Moisture contents, determined by loss-on-drying at 102°C, were 0.79%, 3.68% and 5.32%, respectively. The formulation used for granulation consisting of 72% lactose, 24% MCC and 4% HPC was blended at 20 rpm for a duration of 10 minutes in an automatic tumbler mixer (Inversina 20L – Bioengineering AG, Switzerland). Water was used as liquid binder. These excipients were deemed suitable for efficient twin-screw processing due to their well-established functionality in wet granulation. Lactose, as a brittle material with fragmenting properties offers improved flowability and good compaction behaviour; MCC is a plastically deformable material with a porous structure that enhances liquid uptake and binder distribution during wet granulation, contributing to granule strength and improved compressibility; the low-substituted form of HPC acts as a dry binder and, due to its swellable nature, supports granule formation under shear forces [32].

### 2.2. Methods

#### 2.2.1. Granulation

Granules were prepared via continuous wet granulation using the ConsiGma<sup>TM</sup>25 (GEA Pharma Systems, Collette<sup>TM</sup>, Wommelgem, Belgium) manufacturing line. The powder blend was manually fed to the loss-in-weight feeding hopper. The process begins with the powder being gravimetrically transferred to the twin-screw granulator at a constant feed rate of 10 kg/h, while the liquid binder was added automatically by a peristaltic pump through two liquid addition ports. Wet granulation was performed at a speed of 400 rpm by two co-rotating screws, with a diameter of 25 mm, a length-to-diameter ratio of 20:1 and a configuration containing two kneading zones separated by one 4-pitches long conveying element. Each zone consisted of 6 kneading elements each at a forward stagger angle of 60°. The liquid mass flow was varied within a suitable operating range and as described in sections 2.2.3.5. and 2.2.3.6. while all other process parameters were kept constant.

#### 2.2.2. Fluid-Bed Drying

The integrated drying unit within the ConsiGma<sup>TM</sup>25 system is a six-segmented semi-continuous fluidised bed dryer, as seen in Figure 1. Each segment is herein referred to as a cell. Following the granulation process, granules were gravimetrically transferred to the first cell for 180 s (filling time) through a so called wet granule inlet tube connecting the twin-screw granulator and the FBD. Fluidisation or drying of granules with hot air begins concomitantly with the filling time. The inlet air flowrate used throughout the experimental procedures was 280 m<sup>3</sup>/h ( $\pm$  5 m<sup>3</sup>/h), the inlet air temperature was 50°C, whereas the drying time was 600 s. As the first cell completes its filling phase, granules are further loaded into the subsequent cell. Unloading of granules occurs after the drying cycle is completed within a specific cell, and dried granules are then pneumatically transported to the milling unit operation. Nevertheless, once unloading is complete, the dryer's filter blow-back system activates, which imposes pushing a compressed air stream through the filter to remove any fines that may be stuck to the cartridge. Three blow-back pulses are activated after the unloading of each cell. A visual representation of fluid-bed's mode of operation is presented in Figure 1. All experiments were performed by starting the granulator at cell 1 to ensure steady-state operation and was paused

after cell 2 filling stage completion to reduce material wastage, meaning that no granules were fed to cells 3 - 6.

Additionally, the ConsiGma™25 continuous manufacturing platform incorporates a digital twin, powered by PharmaMV software platform (Perceptive Engineering Ltd., Daresbury, UK), which serves as a real-time virtual model of the physical process. The system integrates process data with advanced computational tools, enabling enhanced monitoring and control of critical unit operations. In this study, on-line monitoring of the cell temperature via the ConsiGma™25 digital twin was employed as a control strategy to ensure reliable drying conditions across all experiments. After an initial temperature drop caused by wet granule filling, the cell temperature enters a plateau phase, corresponding to the constant rate period, during which surface moisture is removed from the granule bed. This is followed by the falling rate drying period, which further stabilises as the cell temperature reaches values approximate to those of the air inlet temperature. The end of drying was considered complete when the cell temperature stabilised at values approaching the inlet air temperature, indicating that the majority of surface and bound moisture has been removed from the granules.

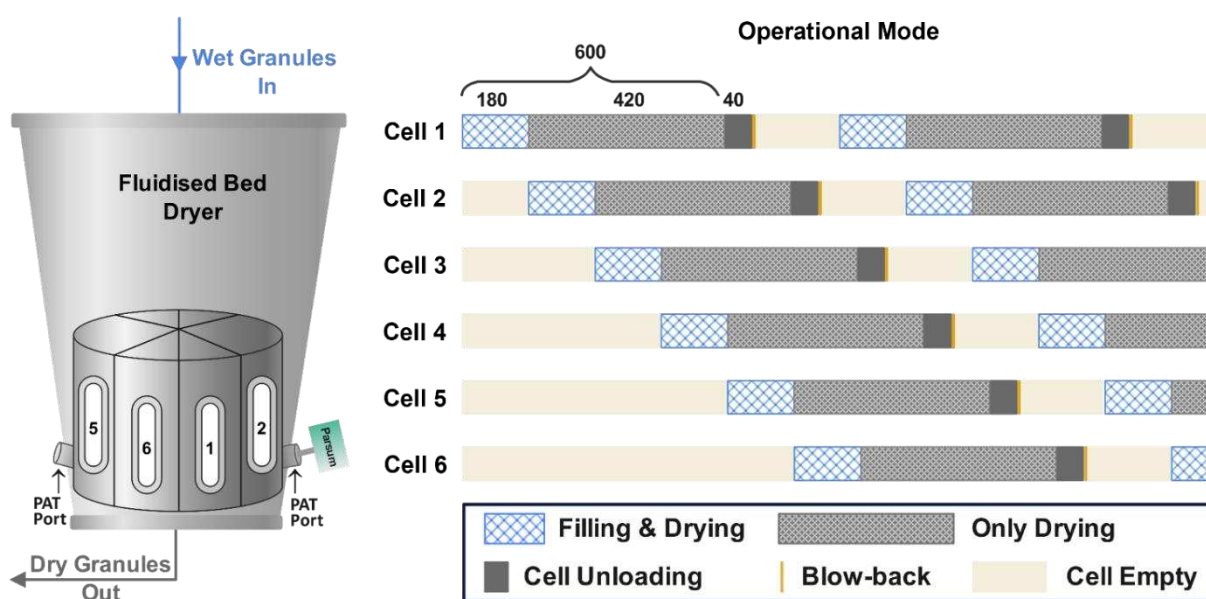


Figure 1 The ConsiGma™25 six-segmented fluid bed dryer depicting the position of the Parsum probe within Cell 2 and its operational mode consisting of filling and drying concomitantly, drying only, cell unloading, filters blow-back and cell empty. The duration of each stage is presented in seconds (s).

## 2.2.3. Granule Size Measurements and Experimental Procedures

### 2.2.3.1. Off-line Granule Size Measurements (Digital Microscopy)

An individual batch of granules was specifically produced for the sole purpose of off-line characterisation. Granules were manufactured using the process parameters presented in section 2.2.1. and with a liquid mass flow of 66.6 g/min (achieving a L/S ratio of 0.4). The twin-screw granulator (GEA Pharma Systems, Collette™, Wommelgem, Belgium) was run for a duration of 3 minutes and wet granules were collected straight after the granulation process. Granules were air-dried for 72 hours. The sample was further manually sieved into various size classes in order to obtain three sub-batches of granules with significantly different sizes.

A reference GSD for each granule sub-batch was determined using a digital microscope (VHX-5000, Keyence, Milton Keynes, United Kingdom). This characterisation method was chosen as a reliable, non-destructive technique that provides information on both the size and shape of the granules. The sample was spread on a glass microscope slide which was placed on a black

background. Granules were manually separated in order to avoid size overestimation caused by granules sticking to each other. The automatic area measurement tool in the VHX-5000 software application (Version 1.3.2.4; System Version 1.04) was used to calculate granules' Feret diameter. Granule boundaries were automatically extracted using the bright area function, which distinguishes the granules from the black background. Brightness thresholds were optimised using the software's extract picker and histogram functions, producing a binary image suitable for dimensional analysis. The Feret diameter was calculated according to the system's definition as the maximum distance between two points on the granule boundary, measured along the 0° or 180° axis. The extracted values were further used for volume-based GSD calculation and each size range was determined based on 20 microscopic images from each sub-batch.

### **2.2.3.2. SFV Granule Characterisation and Data Acquisition**

Real-time granule size measurements were performed through SFV using an IPP70-S probe (Parsum, Chemnitz, Germany). In addition to the probe, the system includes an air supply box connected to an in-lab compressed air source, a PC used for data acquisition. A D24 air dispenser accessory was used in conjunction with the probe. This accessory is suitable for when a high-load granule flow is present and, although it poses a restriction due to its 3.8 mm measurement opening, it must be used to reduce contamination of the optics, avoid accumulation of material on the probe and improve the flow of the granule stream so that accurate measurements are performed. The dispenser was used with default internal (20 L/min) and external (3 L/min) pressurised air flow values. Moreover, the external air flow aiding in granule stream thinning (keeping the optical components clean) implied a timed compressed air pulse to be generated every 15 s for a duration of 2 s. Data acquisition was performed with the aid of a licenced software as part of the IPP70 system. The measurement software used herein was the IPP V9.00, which displays real-time GSD histograms, the volumetric percentiles (Dv10-Dv50-Dv90) and granule rates (the number of validly measured granules per second). The ring buffer length set-point was 50,000 particles and data was recorded every 5 seconds during each experiment.

### **2.2.3.3. In-line Moisture Content Measurements (NIR)**

As granules' size and subsequent behaviour during fluid-bed drying is also directly related to their moisture content, an in-line FP710e near-infrared (NIR) spectroscopy probe (NDC Technology, Dayton, Ohio, USA) was used to detect granules' moisture content post drying for further validation. The probe was installed after the FBD and prior the milling unit operation. The average moisture content and standard deviation of the entire mass of granules unloaded from a specific cell were automatically displayed on the ConsiGma<sup>TM</sup>25 twin interface and recorder for each in-line experiment performed.

### **2.2.3.4. Benchtop Experiments**

For the purpose of evaluating the effect of coincidence occurrences using elongated granules on the volumetric percentiles (Dv) obtained through SFV sensory measurement, the IPP70-S probe was installed on a laboratory benchtop as depicted in Figure 2. For each individual benchtop experiment 10 g of each granule sub-batch subjected to digital microscopy was fed to the probe's field of measurement using a vibrating feeder (DR100, Retsch, Haan, Germany). Granules were dispersed by means of pressurised air as presented in section 2.2.3.2. Both a low and a high feed rate was applied for each of the three individual sub-batches of granules, resulting in a total of six experimental runs. The granule mass feed rate was varied from 1.32 to 15 g/min, depending on the sub-batch used.

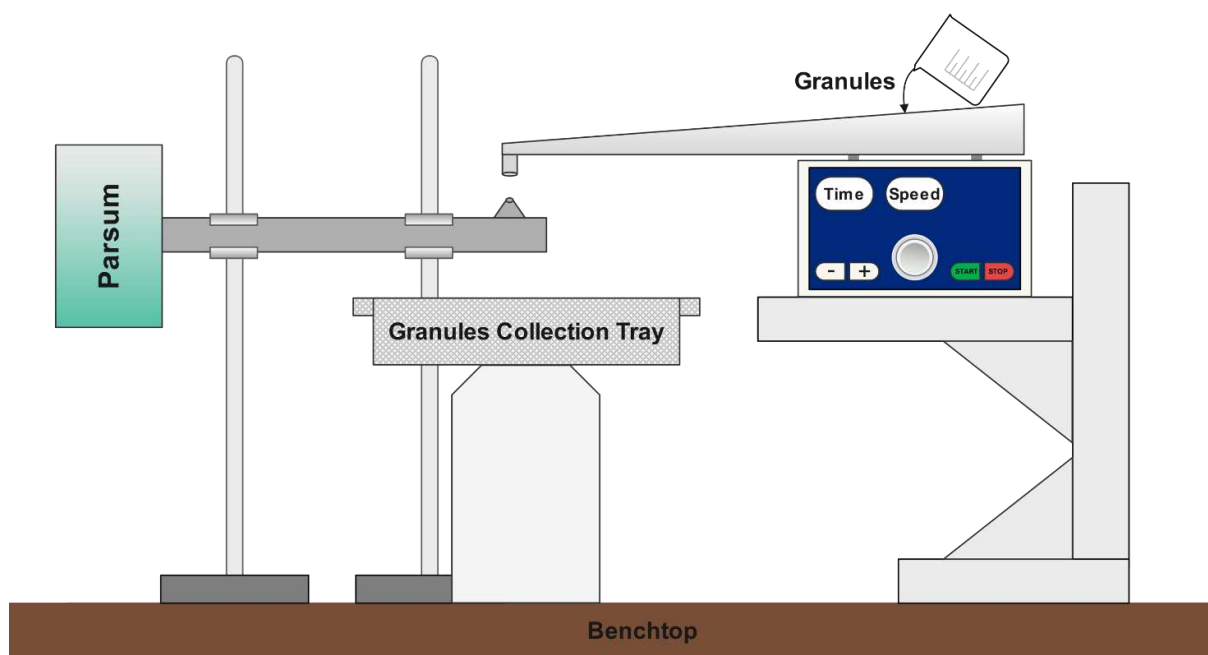


Figure 2 Schematic diagram of the off-line benchtop experiments set-up depicting the vibratory feeder position in relation to the Parsum probe for the determination of coincidence levels.

### 2.2.3.5. ConsiGma™25 In-line Experiments

To achieve a complete understanding of granules' patterns based on size and rate during fluid-bed drying, and ultimately to establish a reference granule behaviour that aids in rapid detecting potential in-process disturbances in CPM, granules have been characterised in real-time using the in-line IPP70-S probe (Parsum, Chemnitz, Germany). The probe was installed within the fluid-bed's cell 2, which incorporates a PAT port (Figure 1). The probe was inserted at a length of 20 cm within the PAT port and an angle to the horizontal of 20°, being positioned approximately 5.5 cm above the distributor plate.

The first set of in-line experiments were carried as independent real-time measurements, where only the L/S ratio was varied while all other parameters – including the powder feed rate – were kept constant. Three L/S ratios were investigated, namely the lower boundary of 0.15, an intermediate value of 0.3 and the upper limit of 0.4. To achieve the desired L/S ratio, only the liquid mass flow was varied such as: 25 g/min, 50 g/min and 66.6 g/min respectively. This range has been selected as a suitable operating space, based on both the ConsiGma™25 standard operating procedure and previous studies on continuous manufacturing [33–35]. The low and high L/S ratio boundaries were deliberately chosen to assess system's responsiveness when producing granules of significantly different sizes, and most importantly due to the differing water-binding characteristics of the formulation's primary excipients. Each experiment was performed in triplicate to ensure reproducibility.

The feasibility of operating across wide L/S ratio boundaries in twin-screw granulation of formulations containing lactose and MCC is attributed to materials' complementary physicochemical properties. The wettability characteristics of the formulation excipients are known to influence liquid distribution and granule formation [32]. This topic has been extensively studied in the literature across different applications, with techniques such as the contact angle measurement, the drop penetration time method or the surface free energy analysis being well-established methods for assessing powder wettability [36–40]. As a water-soluble excipient, lactose promotes binder distribution through partial dissolution at low L/S ratios and facilitates liquid bridge formation at higher L/S ratio [41]. In contrast, MCC's porous structure and hygroscopic nature allow for strong capillary interactions with the

granulation liquid, reducing the amount of free liquid required for effective granule formation, while simultaneously supporting granule consolidation through plastic deformation [32]. Additionally, the low-substituted HPC, with its intense water uptake characteristics, contributes through its swelling capacity and porous morphology to enhanced water retention and supports particle agglomeration [42]. This combination allows for robust granule formation across a broad L/S ratio range. Additionally, based on experimental findings (see Section 3.3.1.3.), exceeding the upper limit would cause the production of highly cohesive granules, resulting in inefficient fluidisation and further negatively impacting process stability.

#### **2.2.3.6. ConsiGma™25 In-line Sudden L/S Variation**

Additional experiments where the L/S ratio was varied in-process, while all other granulation and drying conditions are kept constant were carried. The change in L/S ratio was performed at a constant powder feed, meaning that only the liquid mass flow was varied during processing. This methodology involved starting the granulator using a high liquid mass flow of 66.6 g/min for a duration of 60 s, after which the mass flow was varied to the lower margin of 25 g/min and was run for a duration of 120 s as observed in Figure 3. Through this approach a sudden irregularity within the system was mimicked, as high fractions of coarse granules achieved through using a L/S ratio of 0.4 were initially fed to the FBD, after which an increased number of fine granules were produced using a low L/S ratio of 0.15. The experimental procedure was performed in triplicates. The size range of < 200 µm and > 1600 µm was selected to characterise the fine and coarse granules, respectively. This selection was based on the powder blend's Dv95 value of 192 µm, ensuring a representative assessment of the chosen lower limit. Additionally, it is known that the ConsiGma™25 continuous system employs a milling unit operation following the FBD (section 2.2.2.). Although not a part of this work, since milling ensures that granules fall within a specific size range for accurate compression using a mesh with 1.575 mm diameter openings, the selected upper limit was deemed suitable for the purpose of this paper.

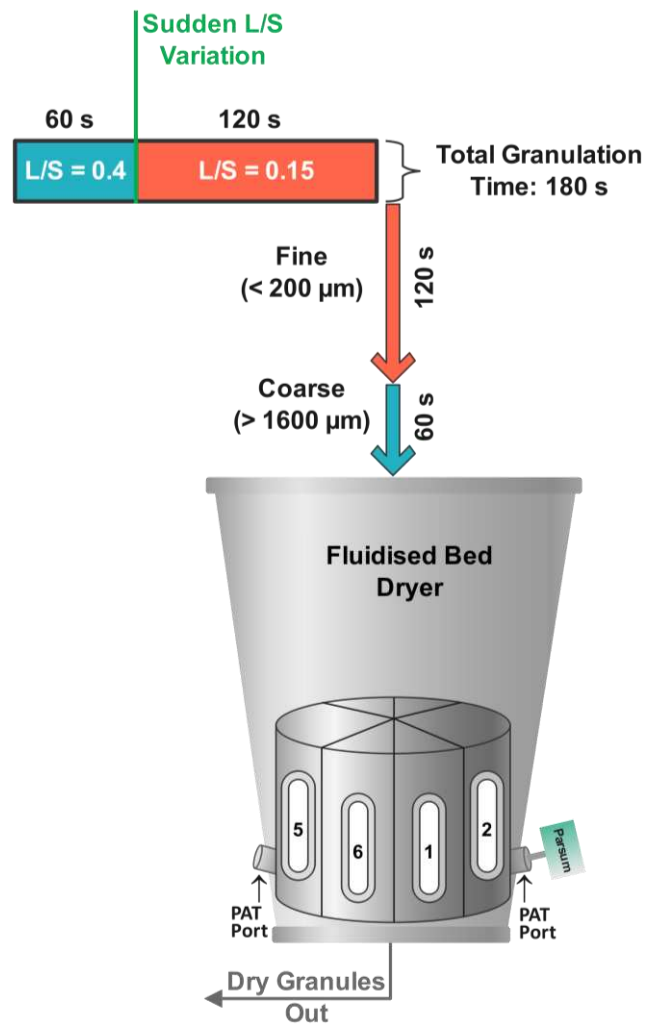


Figure 3 Schematic representation of the secondary experimental procedure where irregularities within the system were mimicked through varying the L/S ratio from the higher limit (0.4) to the lowest value (0.15) without stopping the granulator. The experimental procedure was performed in triplicates and granules' CQAs were investigated in real-time using the SFV Parsum probe inserted in fluid-bed's cell 2.

### 3. RESULTS AND DISCUSSION

#### 3.1. Off-line Granule Characterisation (Digital Microscopy)

The sieved granules selected for the benchtop experiments were firstly subjected to reference size measurements using digital microscopy for the purpose of categorising three various sub-batches (SB1, SB2 and SB3) in significantly different size classes. The selection of samples across various size ranges aimed to ensure that coincidence instances (granules overlapping) resulting in GSD overestimation occurred irrespective of the granule size when using the Parsum probe.

The microscopic images presented in Figure 4 visually confirm the variability in size in between samples. Additionally, it can be seen that granules produced using a twin-screw granulator are mostly elongated or irregularly shaped. To quantify the particle shape, the circularity index (C) was calculated for each sub-batch based on the data obtained from digital microscopy. The circularity is defined as [43]:

$$C = \frac{4\pi A}{P^2} \quad (2)$$

where A is the projected area and P is the perimeter of each granule. In this case, a value of 1 corresponds to a perfect circular shape, whereas a lower value indicates deviation from circularity, reflecting a higher degree of elongation or irregularity of granule shape. A statistical summary of the circularity index for each sub-batch was performed using IBM SPSS Statistics (Version 29) and is presented in

Table 1. A one-sample t-test revealed that all three sub-batches exhibit statistically significant deviations from a perfect circular shape ( $C = 1$ ), with  $p < 0.001$  in all cases. To quantify the degree of these differences, Cohen's  $d$  – expressing the difference between the sample mean and the reference in standard deviation units – was obtained (where  $|\text{Cohen's } d| > 0.8$  denotes large effects). The effect sizes show large negative values, indicating substantial practical deviations from circularity. Hence, the results confirm that the granules are significantly non-circular, supporting the need to consider shape effects when performing volumetric size estimations.

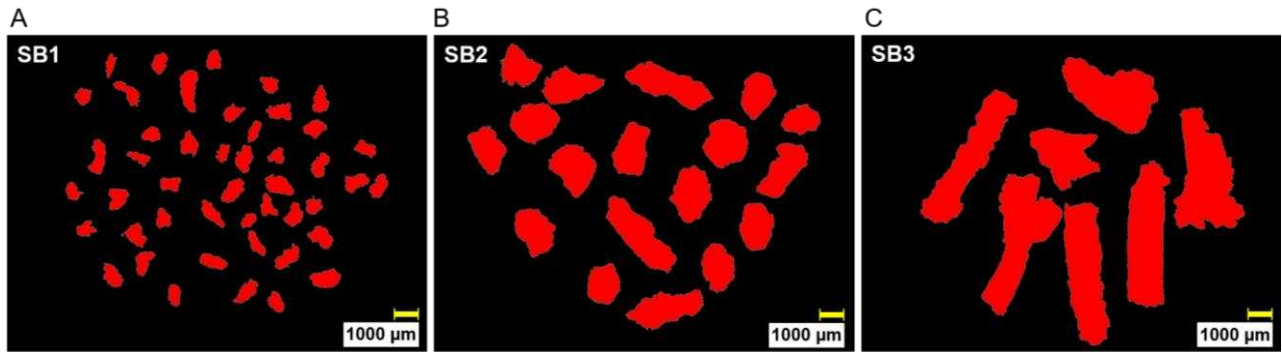


Figure 4 Photomicrographs depicting examples of granule size and shape depending on the sub-batch investigated and used for the determination of granule size distributions with the aid of the automatic area measurement tool. Scale bar: 1000  $\mu\text{m}$

Table 1 Statistical evaluation of granules' shape using circularity index for three sub-batches of granules (SB1, SB2 and SB3) used for benchtop experiments and the associated effect size analysis (Cohen's d).

	<b>Mean Circularity Index <math>\pm</math> SD</b>	<b>Min</b>	<b>Max</b>	<b>Cohen's d</b>	<b>p-value</b>
<b>SB1</b>	0.52 $\pm$ 0.11	0.18	0.84	-4.06	< 0.001
<b>SB2</b>	0.51 $\pm$ 0.10	0.27	0.76	-4.87	< 0.001
<b>SB3</b>	0.54 $\pm$ 0.10	0.25	0.74	-4.15	< 0.001

To further evaluate the influence of granule shape on volume-based size estimations, the density and cumulative distributions generated for each individual sub-batch of granules under both spherical and ellipsoidal assumptions are presented in Figure 5 A-D. For relevance to the benchtop experiments presented in section 3.2, granule's Feret diameter – obtained as presented in section 2.2.3.1 – was used to determine the reference volume-based distributions. The reason for selecting Feret's diameter for the development of the current GSD is due to the fact that this parameter represents a direct measurement of the granule's size along specific orientation [44], similar to the chord length distance which is used by the Parsum probe.

As observed in Figure 5 A and C, the density distributions show that the samples selected contain high fractions of either small (SB1), intermediate (SB2) or large (SB3) granules under both spherical and ellipsoidal assumptions. Undoubtedly, the cumulative distributions shown in Figure 5 B and D express the same pattern for each sample set, as expected. By determining the cumulative distribution, the statistical Dv percentile values of interest showing a certain percentage of the volume of sample with sizes lower than the chosen point can be derived. The extracted Dv10, Dv50 and Dv90 under both spherical and ellipsoidal assumptions are presented in Table 2. To assess whether the choice of geometric model (spherical or ellipsoidal) significantly influences the percentiles of interest, statistical analysis was performed. Since the difference between the Dv values (DvEllipsoidal - DvSpherical) did not follow a normal distribution, the Wilcoxon signed-rank test was used to compare the values from the two models. The results indicated no statistically significant difference ( $p = 0.515$ ) between the Dv values obtained under spherical and ellipsoidal assumptions.

However, it is anticipated that the extracted Dv percentile values under both models are slightly larger than the actual size of the granules. As previously mentioned, and as depicted in Figure 4, the majority of granules used for this measurement are irregularly shaped or elongated, rather than perfectly spherical or ellipsoidal, which leads to a slight overestimation of their actual size. Furthermore, the Feret diameter measures the longest distance between two points that are tangent to granule's boundaries [44], while the chord length used by the probe represents the distance between two connecting points on the edge of granule's projected area [19]. Thus, the Feret diameter is expected to be larger than the chord (see Table 3) – unless the chord happens to coincide with granule's longest span or if the granules are perfectly spherical.

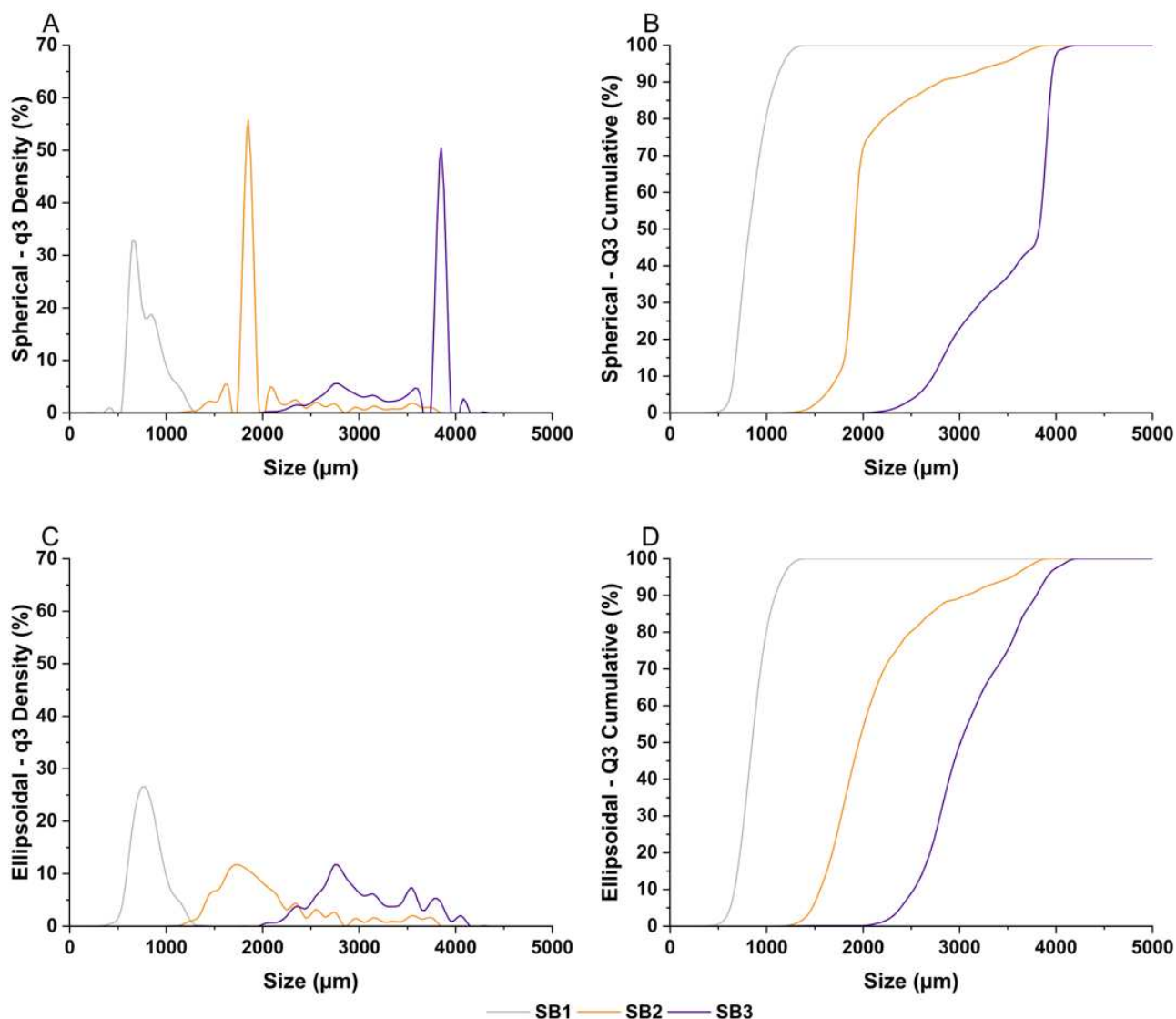


Figure 5 Volumetric density and cumulative distributions under A – B: spherical and C – D: ellipsoidal assumptions for granules produced specifically for the benchtop experiments based on data obtained using digital microscopy. The distributions were calculated using 20 microscopic images for each sub-batch investigated (SB1, SB2, SB3).

Table 2 Comparison of volume-based percentile values (Dv10, Dv50, Dv90) for reference granules under spherical and ellipsoidal assumptions based on digital microscopy.

Reference Granule Size ( $\mu\text{m}$ )						
Spherical Assumption (DvSpherical)				Ellipsoidal Assumption (DvEllipsoidal)		
	Dv10	Dv50	Dv90	Dv10	Dv50	Dv90
<b>SB1</b>	669	817	1086	675	847	1085
<b>SB2</b>	1738	1912	2797	1558	1954	3048
<b>SB3</b>	2729	3854	3934	2530	3008	3795

### 3.2. Benchtop Experiments

The Dv10, Dv50, Dv90 values, alongside the granule rate with time for benchtop experiments obtained using the Parsum probe are presented in Figure 6 A-F. An average granule rate – describing the validly measured particles passing through the probe’s measurement field per second – for each sub-batch investigated and depending on the feeding rate (low or high) is presented in Table 3. It can be clearly observed that as the granules’ size increases, the overall granule rate decreases. This is due to the fact that the experiments were performed using a constant mass of granules (10 g) regardless of the sub-batch investigated. It has been previously demonstrated that the samples selected contain high fractions of either small (SB1), intermediate (SB2) or large (SB3) granules (section 3.1.). Provided that the granule mass is constant, large granules account for a greater portion of the mass due to the directly proportional relationship between mass and volume. Hence, when investigating samples containing granules that fall within various specific size classes, it is expected that the number of granules decreases with an increase in size and thus, volume. By having a reduced number of granules within the same mass, the rate of granules passing through the probe’s field of measurement decreases as well.

The granule size percentiles at low granule rates can be observed for each of the three sub-batches investigated in Figure 6 A (SB1), C (SB2), E (SB3). The size is seen to be in good agreement with the reference measurements presented in Table 2, although a slight difference is observed, with larger values determined using the microscope technique as expected. To quantify this, relative deviations reflecting the degree of difference in size when comparing the spherical and ellipsoidal model-derived Dv percentiles to the Parsum benchtop measurements are presented in Table 3. Across all sub-batches, both geometrical assumptions show positive deviations. While the ellipsoidal model present lower deviations for SB3 and at Dv10 for SB2, the spherical model shows slightly lower deviations at Dv10 and Dv50 for SB1. This further highlights the limitations of both model assumptions when compared to the Parsum measurements, and thus, the Dv volumetric values previously presented in Table 2 should serve as reference information used to categorise each granule sub-batch subjected to benchtop experiments.

Table 3 Relative deviation (%) of granule’s percentiles (Dv10, Dv50, Dv90) under spherical and ellipsoidal assumptions compared to the benchtop Parsum measurements at low granule rates and the corresponding average granule rates recorded by the Parsum probe under low and high feed rate conditions.

	Relative Deviation (%) (Spherical)			Relative Deviation (%) (Ellipsoidal)			Average Granule Rate (1/s) ± SD	
	Dv10	Dv50	Dv90	Dv10	Dv50	Dv90	Low	High
<b>SB1</b>	48.00	23.41	12.19	49.33	27.94	12.08	17.05 (± 4.85)	64 (± 38.19)
<b>SB2</b>	60.62	19.79	9.47	43.99	22.43	19.29	6.87 (± 2.39)	16.44 (± 10.96)
<b>SB3</b>	41.91	54.34	19.24	31.56	20.46	15.03	2.66 (± 1.45)	8 (± 3.8)

In terms of the effect of granules overlapping on the Dv percentiles, Figure 6 B (SB1), D (SB2), F (SB3) demonstrate that coincidence instances do occur when high granule rates are used, as compared to the same measurements at low granule rates for each sub-batch. The granule size overestimation as a result of granules’ overlapping seems to especially impact the Dv90 values. To quantitatively assess the impact of feed rate on Dv90 values, statistical analysis was performed for each sub-batch. The results presented in Table 4, show that Dv90 values are significantly higher at high feed rates than at low feed rates across all experiments (Mann-Whitney U test,  $p < 0.006$ ). This confirms that overestimation occurs at higher feed rates, with absolute differences in mean Dv90 ranging from 55 – 461  $\mu\text{m}$  between samples.

Additionally, the extent in overestimation becomes more pronounced as the granule size increases, with percentage differences in mean Dv90 values of 5.68% for SB1, 13.38% for SB2 and 13.97% for SB3. This is due to the fact that as the probe observes two or more granules as being one within a population, the entire distribution is shifted towards a higher fraction of coarse granules. As the granules' size and volume increases, the overestimation also becomes more pronounced due to a larger overall apparent volume being detected compared to the overlapping of smaller granules. Furthermore, as a result of the cumulative distribution being shifted towards larger granules, the Dv10 and Dv50 percentiles are slightly underestimated in each case, although this difference is not as apparent as in the case of Dv90 due to large granules dominating within a volume-based distribution.

Table 4 Statistical comparison of benchtop experiments Dv90 values between low and high feed rate conditions for three various granule sub-batches. Statistically significant differences (p-value < 0.05) indicate the impact of feed rate on the granule size percentile measurement.

	<b>Feed Rate</b>	<b>Mean Dv90 ± SD (µm)</b>	<b>Absolute Difference in Mean (µm)</b>	<b>*p-value</b>
<b>SB1</b>	Low	968 ± 111.86	55	0.006
	High	1023 ± 476.71		
<b>SB2</b>	Low	2555 ± 289.61	342	0.006
	High	2897 ± 1523.64		
<b>SB3</b>	Low	3299 ± 450.88	461	< 0.001
	High	3760 ± 1323.11		

\*p-values derived from Mann-Whitney U due to non-normality of data. Normality was assessed using the Shapiro-Wilk test; p < 0.05 was observed for most groups, indicating deviation from a normal distribution.

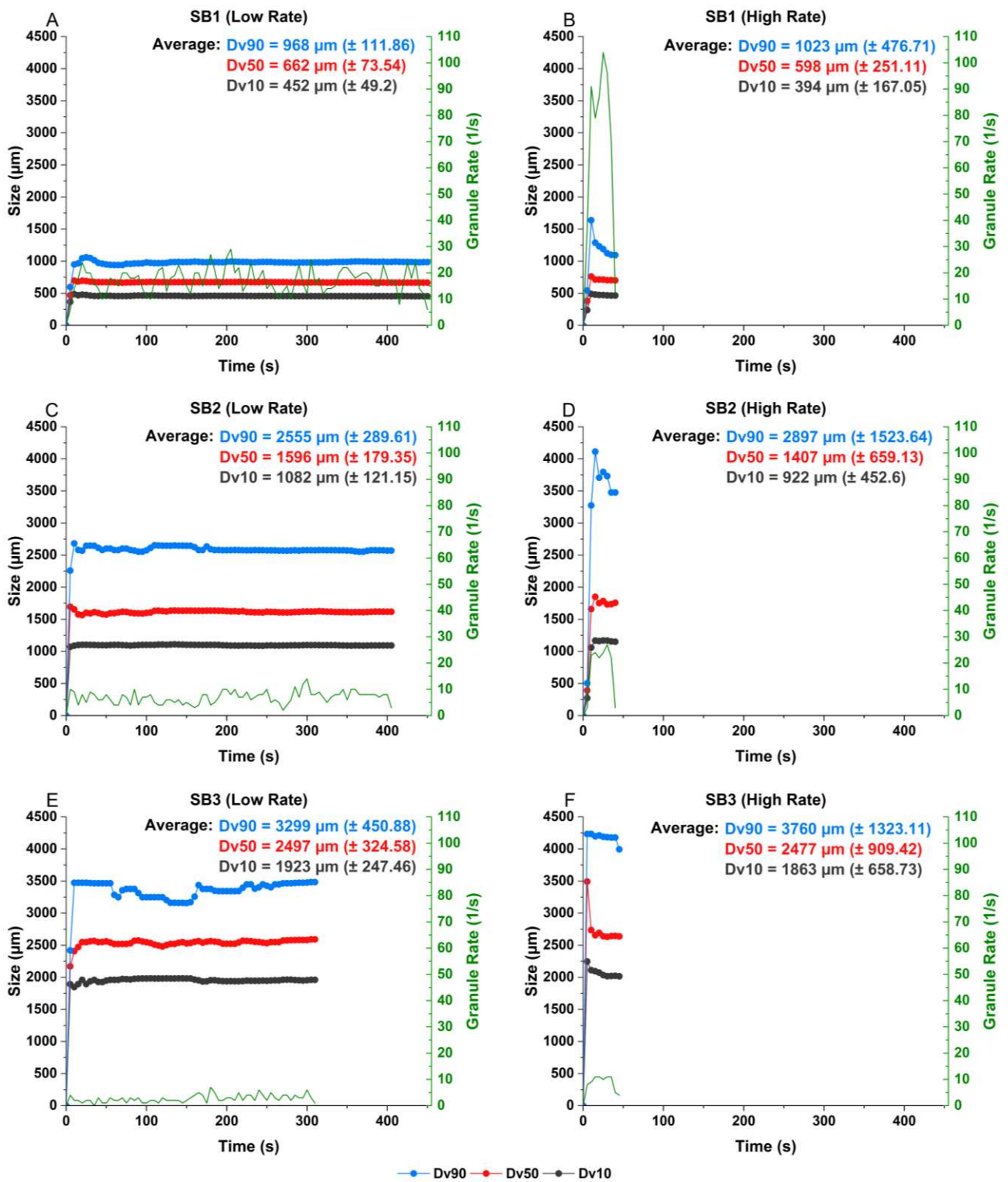


Figure 6 Percentile D volumetric values (Dv10, Dv50, Dv90) of the benchtop experiments using the Parsum probe for three various granule sub-batches at different granule rates depicting the number of validly measured granules per second (See Table 3 for average granule rates for each measurement).

### **3.3. ConsiGma™25 In-line Granule Characterisation**

#### **3.3.1. Individual L/S Ratio Variation**

##### **3.3.1.1. Volumetric Granule Percentiles (D<sub>v</sub>)**

With a main focus on developing a comprehensive understanding of granules' size and behaviour in real-time, this section provides an analysis of the widely used volumetric characteristics during one of the most important unit operations as part of a continuous system – the segmented fluid-bed dryer. The real-time D<sub>v</sub> sizes (D<sub>v10</sub>, D<sub>v90</sub>, D<sub>v50</sub>) for granules produced under three various L/S ratios, namely the lower limit of 0.15, the intermediate 0.3 and the upper boundary of 0.4, throughout the entirety of the fluid-bed drying process are presented in Figure 7 A-C. The completion of the filling stage (180 s) has been referenced in each graphical representation. Generally, the granule volumetric size exhibits considerable variation depending on the L/S ratio employed during granulation for each D<sub>v</sub> value considered, with larger granules being produced as the L/S ratio is increased.

The filling phase, defined throughout the first 180 s process time, exhibits size fluctuations at each L/S ratio (Figure 7 A-C). At this stage, granules are being gravitationally fed into the FBD through a “wet granule inlet tube” located at the top of the cell. At the same time, hot air pushes the granules entering the bed upwards. Moreover, granules produced through twin-screw granulation usually exhibit size distributions characterised as being bimodal (see Figure 12). A bimodal distribution indicates that two peaks are observed in the representation, which suggests that high fractions of both small and large granules exist within a population. Hence, considering that granules of various sizes travel through the fluidised bed under gravitational forces, the drag forces acting on the particles will differ depending on their size. On this basis, smaller granules are anticipated to reach their settling velocity faster as compared to the fraction of coarser granules.

Additionally, differences in granule size within a population may lead to the formation of trajectory segregation. This phenomenon implies that the dynamics of particle movement through the fluid is highly dependent on their size, leading to granule separation along different paths during feeding [45]. This causes the granules to follow a trajectory that favours the detection of slightly larger agglomerates during the incipient phase of filling. It can also be considered that, as a multiple particle system, particle-particle interactions – caused by a high number of granules flowing through the bed in close proximity to each other – might occur, resulting in each granule's movement being impacted by the presence of another granule. Nonetheless, particle-wall collisions can also influence granules' dynamics as they interact with the FBD's walls, leading to possible alterations in their velocity and movement. Consequently, granules' behaviour becomes erratic, which further contributes to the size fluctuation observed during the filling phase in each case investigated. A more comprehensive analysis of granules' size and behaviour throughout the remaining drying time-period in real-time, taking into account various granule characteristics and the influence of systematic process factors, is provided in section 3.3.1.2 and 3.3.1.3.

Overall, it can be observed that although both the D<sub>v10</sub> and D<sub>v50</sub> values show limited fluctuations with time, the D<sub>v90</sub> displays nearly identical values for long time-periods with abrupt changes at various points in time. This tendency is firstly observable at the lowest L/S ratio of 0.15, during the filling stage for a duration of 60 s. When higher L/S ratios are applied this behaviour becomes more apparent and subsists for longer periods especially after the filling process concludes, as seen in Figure 7 B and C. Additionally, it can be seen that in the case of granules produced under the highest L/S ratio of 0.4 (Figure 7 C), large D<sub>v90</sub> values of up to 5000 μm were measured, despite the probe's dispenser opening of only 3.8 mm diameter. This is due to the fact that during twin-screw granulation, elongated granules are formed, as seen in Figure 4. These elongated agglomerates can pass vertically

across the measurement field and fit through the 3.8 mm opening, even if their longest dimension exceeds the diameter of the dispenser.

The Parsum IPP70-S probe utilises the principle of SFV, a well-established method for in-line granule size measurement. In this technique, granules passing through the probe's laser beam cast a shadow that interrupts the light reaching a linear array of optical fibres. The duration of each interruption corresponds with the granule size, while the sequence of interruptions provides information about their velocity [19,20]. The resulting signal pulse conferred by the granule passing through the measurement optic, further used to determine granules' size, might however be impacted by the detection of multiple significantly large granules or a high number of granules.

Although the Dv90 values shown in Figure 7 C remain within the probe's specified measuring range of 50 – 6000  $\mu\text{m}$ , unchanged values are observed over extended periods, as previously mentioned. This behaviour may indicate signal saturation, which can occur when the signal intensity generated by multiple overlapping granules – or by particularly large granules which fit through the measurement opening in a vertical orientation and coinciding with others – exceeds the upper range limit of 6000  $\mu\text{m}$ . Signal saturation might further impact the system's capacity to process data accurately. When a high concentration of granules passes through the laser beam, overlapping shadows may form, thereby reducing the detector's ability to distinguish individual granules. Such interference leading to detector saturation, can result in the display of a previously detected granule's Dv90 that lies within the specified range for long time-periods. Lastly, sudden significant variations in Dv90 after long periods of constant values are detected, which highlight potential downsides such as limited sensitivity or delayed response in accurately displaying this percentile.

Nonetheless, it was previously determined during the benchtop experiments presented in section 3.2., that the occurrence of granules overlapping when using the Parsum probe often arises at higher granule rates. Considering that in-process continuous measurements exhibit significantly high granule rates (see Figure 9), these implications must be avoided when monitoring continuous processes for quality assurance purposes. Hence, further analysis will focus solely on the Dv50 percentile in real-time, as the impact of granules' overlapping on this characteristic is minimal, with a relatively constant behaviour with time as compared to the Dv90. Additionally, as the Dv10 percentile only focuses on the 10% fraction of undersized granules present within the population, the most representative metric for an in-depth understanding of granules' behaviour is the median Dv50. Accounting for the point at which half of the granules are smaller and half larger than the chosen value, the Dv50 confers the most indicative interpretation of the overall behaviour of granules during fluid-bed drying. With an equivalent focus for the entire granule population, the Dv50 is considered a more reliable characteristic for the purpose of this paper.

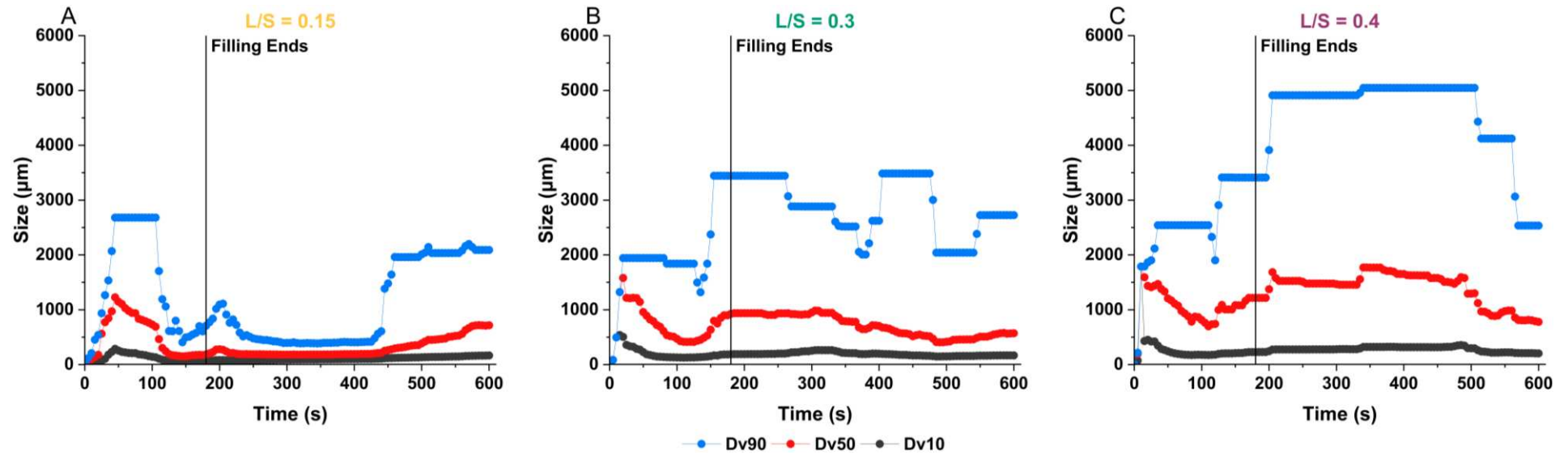


Figure 7 The percentile Dv values (Dv10, Dv50, Dv90) of in-line real-time measurements using the Parsum probe for granules produced under three individual L/S ratios – A: the lower limit of 0.15, B: the intermediate 0.3, and C: the upper limit of 0.4 – throughout the entirety of the fluid-bed drying process.

### 3.3.1.2. Real-time Dv50 Characterisation and Behavioural Patterns

Figure 8 shows the real-time averaged Dv50 percentiles for granules produced at three individual L/S ratios, namely 0.15, 0.3, and 0.4, based on three experimental replicates. As mentioned in section 3.3.1.1., the cell loading duration shows an erratic behaviour in terms of granule size for each variable, caused by numerous factors such as the combination of concurrent processes (filling and drying), the GSD bimodality characteristic to twin-screw granules, interparticle and surface interactions or systematic aspects. As cell filling concludes (180 s) and the fluidisation exhibits fewer fluctuations, a positive relationship between the L/S ratio and granules' size is observed. As a general trend, the granule size increases at higher L/S ratios, which is caused by the increase in liquid feed rate during granulation. When larger amounts of liquid binder are used, a greater number of liquid bridges are formed between primary particles, leading to the formation of larger agglomerates [7,13,14,16].

Taking into account the bimodality of twin-screw granules, it is important to acknowledge that high fractions of fines are typically produced at low L/S ratio, while larger proportions of coarse granules are expected at high L/S ratios. However, granules of various other sizes are still present within the population, regardless of the L/S ratio used. Hence, as the drying process advances, slight Dv50 variances are detected for each parameter. This behaviour is highly dependent on the size of individual granules passing thorough the field of measurement at certain points in time. Furthermore, at 420 s during cell 2 drying, it can be inferred – based on fluid-bed's operational mode (Figure 1) and the process parameters presented in section 2.2.2 – that cell 1 is completing its drying process. Granule unloading from this specific cell proceeds, followed by the activation of the blow-back system 40 s after unloading starts. Removing the granules present in cell 1 increases the air velocity responsible for drying, as the total mass of granules undergoing drying is reduced. This, in turn, enhances the energy available for the system to perform the drying process, improving the fluidisation of the granules in cell 2. As a result, granules' dynamics is enhanced, leading to slightly increased Dv50 variances due to a greater number of granules of various sizes passing through the probe's measuring field approximately 420 s into the process, as depicted in Figure 8.

Considering all the aforementioned aspects that influence granule's behaviour during drying, the Dv50 values recorded between 200 and 400 seconds were deemed the most representative for characterising the entire batch of granules investigated. This is based on the fact that the overall mass of granules present within the fluid-bed and hence particle's position relative to the probe should not significantly vary throughout this time-period. On this basis, it is considered that the granules present in cell 2 are fluidised at a steady rate as no further external operational process, such as cell 1 unloading or the activation of the blow-back system, that might significantly impact granules' movement arises. This time-range (200 – 400 s) will further be referred to as the “stable region”.

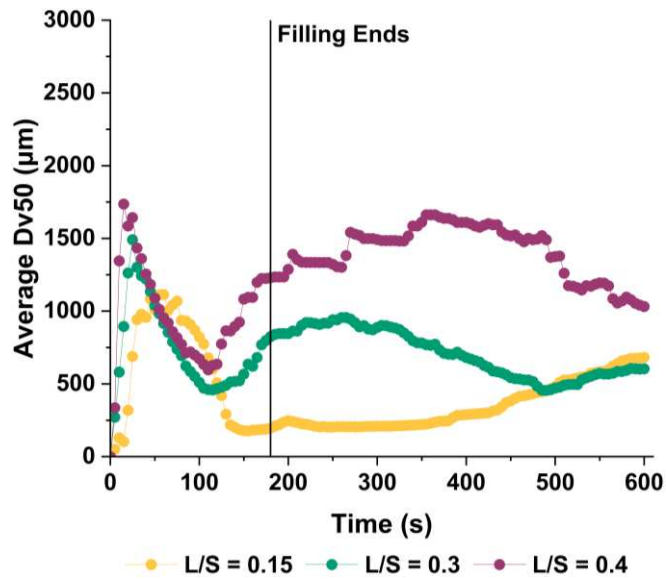


Figure 8 Real-time average Dv50 percentiles for granules produced at three various L/S ratios (0.15, 0.3 and 0.4) throughout the fluid-bed drying process as part of a continuous system. Each average was calculated based on three experimental replicates.

### 3.3.1.3. In-line Granule Rate and the Impact of Granules' Moisture Content

By in-line monitoring of the real-time granule rate during continuous fluid-bed drying, the granules' behaviour can be characterised more in-depth. Figure 9 shows the average granule rate over time for each individual L/S ratio investigated, based on three experimental repetitions for each variable. Additionally, the probe's cleaning system, which uses a systematic upward stream of pressurised air to keep the optical components free of debris, causes the methodical drop in granule rate observed throughout the entire drying process for each L/S ratio investigated.

At a L/S ratio of 0.15 it can be observed that the rate of granules increases significantly as the filling process advances (Figure 9), with approximately 300 granules/s at the start of filling and reaching up to 2500 granules/s at 180 s. This is an expected trend as material is continuously loaded into the dryer during the filling stage, leading to an increase in the overall number of granules within the cell and consequently enhancing the number of particles that enter probe's optical field. However, as cell filling completes, the rate gradually decreases with time. This is due to elutriation/settling, a phenomenon that highly depends on granule's size and density. Although bimodal granules are produced, when using low L/S ratios the number of large granules is significantly lower than the finer granules. With fines having an inherently reduced settling velocity as compared to the larger granules, it is expected that a greater proportion of small granules are pushed towards the top part of the cell and away from the probe during the drying process. Hence, the granule rate is minimal especially towards the end of the process, caused by the detection of the slightly larger agglomerates that remain in probe's proximity during fluidisation.

For the coarse granules produced at the highest L/S ratio of 0.4, the overall granule rate presented in Figure 9 is rather minimal throughout the entirety of the filling process (with a maximum of 270 granules/s). In order to obtain a L/S ratio of 0.4 the liquid addition flowrate used during granulation was 66.6 g/min. This further causes each individual granule to contain high water percentages due to the greater number of liquid bridges formed. Hence, Figure 10 A illustrates that, as a result of granules' high moisture content and considering the limited surface area available for drying, almost the entire mass of granules settles at the bottom of the cell. Additionally, towards filling completion, the granule rate decreases to minimal values (Figure 9) as the probe becomes submerged under the granule bed, indicated by the blue dotted line in Figure 10 A – which shows the positioning of the

probe within the cell. Moreover, once the filling process concludes and only fluidisation takes place within the system, instances of channelling occur. In this particular case, Figure 10 B shows the formation of three channels. This phenomenon arises when granules containing high binder amounts settle at the bottom of the cell, creating resistance to the fluidising air. As a result, uneven air distribution across the cell causes some areas of the granule bed to fluidise at a higher rate, while other parts remain stagnant, eventually creating channelling pathways. However, as drying continues, granules' moisture content decreases which allows for an enhanced granule movement, and thus, the overall rate increases approximately 450 s into the drying process as seen in Figure 9. Noticeably, this is an intrinsically opposite granule behaviour as compared to agglomerates produced at the L/S ratio of 0.15, caused by the overall difference in water flowrate utilised during granulation, as described above.

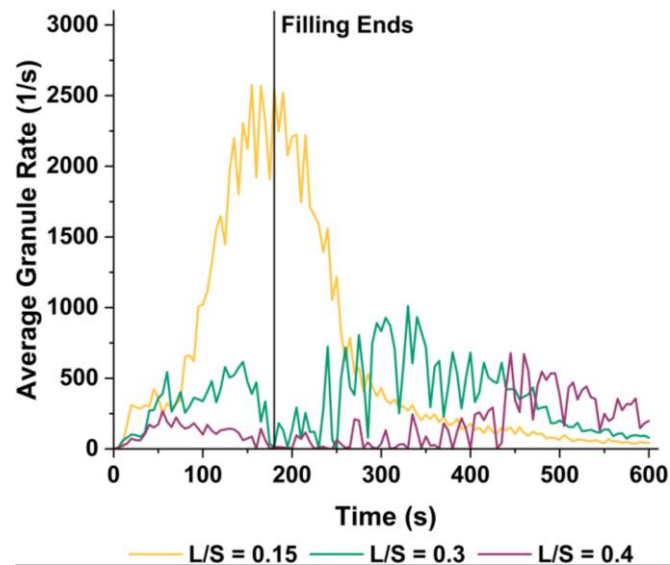


Figure 9 In-line average granule rate measurements, showing the number of validly assessed granules per second, for agglomerates produced under various L/S ratio (0.15, 0.3 and 0.4) during fluid-bed drying. The averages were calculated based on three experimental replicates for each variable.

Additionally, as observed in Figure 9, the granule rate at the intermediate L/S ratio of 0.3 exhibits a combination of behaviours characteristic of both the granules produced at L/S ratios of 0.15 and 0.4. When compared to the highest L/S ratio (0.4), an increased overall granule rate is observed for the intermediate of 0.3. A maximum of 600 granules/s is detected during the filling stage, double the rate previously observed for the L/S ratio of 0.4 throughout this period. Additionally, it is clear that the granule rate at the L/S ratio of 0.3 is considerably reduced compared to the lowest variable (L/S ratio of 0.15) – where the rate reaches a peak of 2500 granules/s during filling. However, as soon as the filling stage is complete, the rate for the L/S ratio of 0.3 granules decreases significantly for a duration of approximately 60 s, as previously observed for the L/S ratio of 0.4. This is caused by some of the granule mass settling at the bottom of the cell which reduces the fluidisation capacity. As the drying process continues the rate increases significantly, indicating a sufficient reduction in granules' moisture content that allows enhanced fluidisation and improved granule detection. Towards the end of drying, a steady reduction in granule rate is observed as previously noted at the lowest L/S ratio of 0.15. At this time granule elutriation/settling occurs, causing the fines to be pushed upwards, with a slightly increase fraction of larger granules being detected during this time.

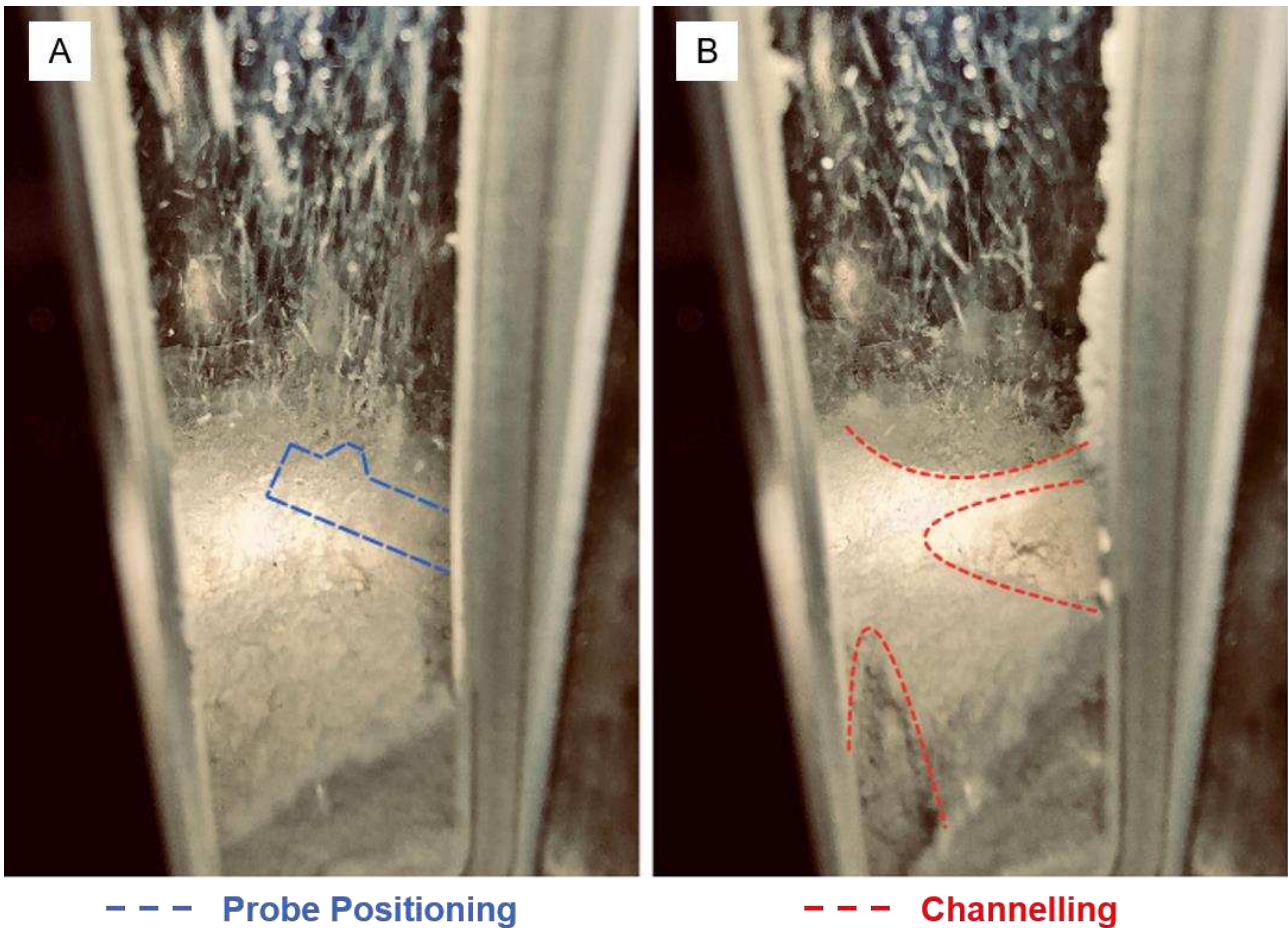


Figure 10 Granules produced using a L/S ratio of 0.4 during fluid-bed drying showing A: granules settling at the bottom of the FBD cell during the filling process and submerging the probe under the granule bed (image captured approximately 170 s into the process), and B: the channelling phenomenon occurring during the drying process (image captured approximately 230 s into the process).

Moreover, to determine the mass of granules loaded into each FBD cell, the process parameters used during the experimental procedures must be taken into consideration (sections 2.2.1. and 2.2.2.). Thus, at a constant powder feed rate of 10 kg/h and a cell filling time of 180 seconds, each experiment contained 500 g of granules in each cell. Since the granule mass loaded into each cell was constant for each experiment (500 g), and based on the total number of granules presented in Table 5 (captured using the Parsum probe throughout the entire drying process - 600 s), it is clear that the number of granules decreases with an increase in L/S ratio. This validates the statement that an increased amount of liquid binder during granulation (with a constant powder feed rate) leads to the formation of more liquid bridges between primary particles, and consequently of larger granules (see Figure 12).

Table 5 Total number of granules captured using the Parsum probe throughout the entirety of the drying process (600 s), based on three replicates performed at various liquid to solid ratios.

L/S ratio	Number of Granules
0.15	78487
0.3	42031
0.4	20018

To further validate the granule rate patterns for each L/S ratio investigated, granules' moisture content was measured using an NIR probe, placed after the FBD and prior to the milling unit operation. Hence, Figure 11 shows the average moisture content attained after drying for granules produced at three various L/S ratios. As expected, a positive relationship showing an increase in moisture content with an increase in L/S ratio is established. This is due to the fact that all drying parameters and the initial powder flowrate were kept constant across experiments, while only the liquid mass flow was increased to obtain higher L/S ratios, as described above.

Generally, with higher L/S ratios granules' moisture content during drying is expected to decrease more moderately and throughout a longer time-period due to the increased bound and surface moisture, as opposed to low L/S ratio granules. Therefore, under constant drying conditions, an approximate linear relationship is observed (Figure 11), which is consistent with the expected trend that higher L/S ratios yield higher residual moisture, up to the limits imposed by the drying process. Given the simplicity of the dataset and the absence of systematic deviation in the residuals, a linear model was deemed sufficient to describe the relationship between granules' moisture content after drying and the L/S ratio. Hence, the previous hypothesis regarding large granules settling at the bottom of the cell due to granules' high moisture content is supported.

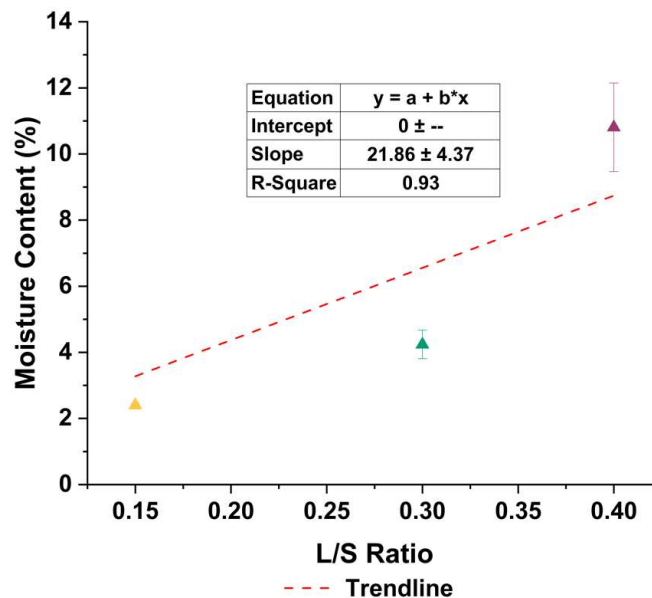


Figure 11 Granule moisture content after drying by means of NIR in-line measurement for each L/S ratio investigated. The data points represent the mean value of three replicates for each individual L/S ratio (The error bars represent the mean standard deviation of three replicates for each individual L/S ratio and which are automatically displayed by the probe).

### 3.3.1.4. Granule Size Distribution at various Processing Times

Figure 12 A-C shows the GSD for granules produced under each L/S ratio at specific time-points during fluid-bed drying, providing an in-depth understanding of how the granules behave as a population during the drying process. As previously established (section 3.3.1.1.), the filling stage induces chaotic granule movement due to multiple factors. At the start of the filling process, herein depicted at 60 s processing time, high fractions of coarse granules  $> 1600 \mu\text{m}$  are detected across all L/S ratio investigated (Figure 12 A-C). Considering the bimodality of twin-screw granules, the premise described in section 3.3.1.1. regarding the occurrence of trajectory segregation during filling is hereby validated. As the filling process continues, the characteristic size for each L/S ratio becomes more apparent. Fines with sizes  $< 200 \mu\text{m}$  dominate the GSD at the lowest L/S ratio of 0.15, while

increasingly larger granules are detected at the intermediate L/S ratio of 0.3 and the highest of 0.4, as expected.

Figure 12 A shows that as the process enters the stable region (200 – 400 s) for granules produced at a L/S ratio of 0.15, the fraction of fines with sizes under 200  $\mu\text{m}$  peaks, reaching a maximum accumulated proportion of approximately 50% at 240 s. The behaviour remains fairly constant until 480 s processing time, when slightly larger granules are being detected by the probe. As stated in section 3.3.1.2., the granules present in cell 1 would have already been unloaded, improving FBD's fluidisation capacity. Consequently, due to the bimodal GSD characteristic to twin-screw granulation and the elutriation/settling phenomena, slightly larger granules are being detected by the probe towards the end of the drying process while fines tend to ascend towards the filters.

For a L/S ratio of 0.3 (Figure 12 B), the stable region shows the detection of larger coarse fractions with a total accumulation of 30% of granules above 1600  $\mu\text{m}$  at 240 s, followed by the detection of slightly larger proportions of fines at 360 s. Towards the end of the process, the proportions of fine and coarse granules shift over time, with 20% fines and 15% coarse at 480 s, and 15% fines and 20% coarse at 600 s. This behaviour proves that elutriation/settling also occurs in this case, as previously stipulated in section 3.3.1.3. The fluctuations observed throughout drying can be attributed to a slightly more pronounced granule bimodality at an intermediate L/S ratio, which results in oscillations in the GSD, as both larger and smaller granules have a somewhat equal probability of being captured at any given point in the process.

In terms of the GSD for granules produced at the highest L/S ratio of 0.4 presented in Figure 12 C, the presence of large fractions of coarse granules is evident. Although it was previously determined that the granule rate at 180 s is minimal (Figure 9) due to the probe being submerged under granules (Figure 10 A), the limited number of granules passing through the probe show a certain increase in coarse fraction compared to the lower L/S ratios investigated. As moisture is gradually removed from the granulated material and the process becomes stable at 240 s, the GSD broadens significantly, with large granules of up to 4500  $\mu\text{m}$  being detected. At this process time the fraction of coarse granules above 1600  $\mu\text{m}$  reaches its highest peak with an accumulated total of 40%. The remaining process time shows a rather constant GSD, with only an insignificant increase in the fraction of fines observed.

Focusing on the overall GSD at each L/S ratio presented in Figure 12 A-C, the difference in granules' behaviour as a population can be effectively highlighted. At the lowest L/S ratio of 0.15, Figure 12 A clearly demonstrates a GSD tendency toward granules under 200  $\mu\text{m}$  (characterised herein as fines), resulting from the reduced amount of liquid binder used during granulation. As the L/S ratio is increased to the intermediate value of 0.3 (Figure 12 B), the GSD becomes concentrated towards median sizes, with only slight fluctuations observed throughout the drying process caused by a more pronounced bimodality. Lastly, the real-time GSD obtained at the highest L/S ratio of 0.4 (Figure 12 C) shows the formation of significantly larger agglomerates due to the increased number of liquid bridges between the primary particles. Hence, Figure 12 A-C successfully demonstrates the behavioural patterns proposed throughout this study, along with the multiple factors influencing the detection and real-time display of granule size during fluid-bed drying. However, it is important to reiterate that the observed granule behaviours are also dependent on the size of the granule detected by the probe at a specific time during the process, as this highly impacts the granule size distributions.

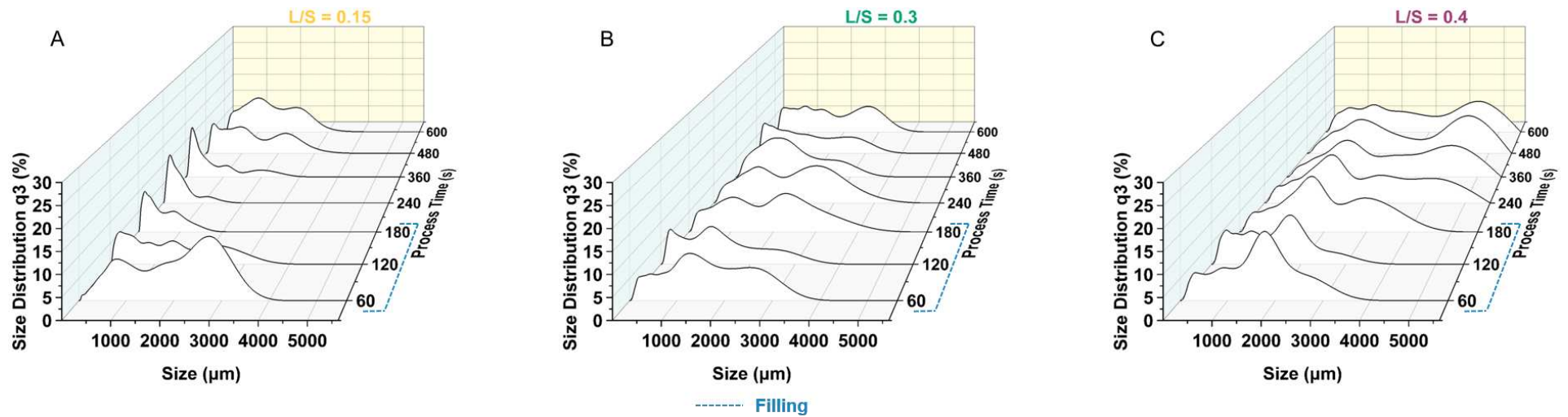


Figure 12 In-line granule size distribution ( $q_3$ ) at various processing times throughout the fluid-bed drying process for granules produced under each individual L/S ratio investigated, namely A: the lower boundary of 0.15, B: the intermediate value of 0.3, and C: the lower margin of 0.4. Each curve represents the average of three experimental replicates at the same processing time.

### 3.3.2. In-process Sudden L/S Ratio Variation

In alignment with the ICH Q13 guidelines [5], which emphasise the importance of identifying and controlling disturbances within the system for enhanced process understanding, additional experiments were performed to address the need for frequent process monitoring. This approach enables the detection of disturbance sources, such as liquid binder fluctuations leading to L/S ratio deviations. To investigate the effects of such irregularities on granules' CQAs, the deviation was mimicked by varying the L/S ratio from 0.4 to 0.15 without stopping the granulator and as presented in section 2.2.3.6. The stability of the powder feed rate and the evolution of the liquid mass flow variation were constantly monitored via the ConsiGma™25 digital twin. Through real-time parameter tracking, it was observed that the transition from the upper to the lower liquid mass flow setpoint occurred gradually over a period of approximately 20 s. Through this variation, no deviation in powder feed rate was observed, thereby allowing for a clear evaluation of the effect of liquid mass flow variation on granules' real-time characteristics. Figure 13 A-B shows the real-time Dv50 percentile and granule rate respectively, for agglomerates produced under a disturbance, compared to the initial reference behaviours for individual L/S ratios of 0.15 and 0.4. The comparison highlights the differences in granule characteristics under normal and disturbed conditions. The in-process L/S ratio change is referenced in each graphical representation (60 s).

In Figure 13 A, the Dv50 values for the disturbed conditions (L/S Change) exhibit a combination of behaviours characteristic to both the 0.15 and 0.4 L/S ratios. During the initial 60 s, a strong correlation with the individual L/S ratio of 0.4 is observed, with large granules being produced, as expected. However, at 60 s, following the induced process disturbance and the transition to the lowest boundary (0.15), a decrease in granule size is detected, falling below the values previously measured at the individual L/S ratio of 0.4. Subsequently, throughout the remaining process time, granules' size remains relatively constant, closely resembling the granules produced under solely 0.15. This trend is expected, considering that the time during which 0.15 granules were filled into the cell (120 s) is twice as long as the 0.4 granules (60 s). As a result, and based on the powder feed rate and the filling time (previously discussed in section 3.3.1.3.), the amount of fines produced at the lowest L/S ratio is significantly higher (333 g) compared to the coarse fractions produced at the highest L/S ratio of 0.4 (167 g). Overall, the sensitivity of the Dv50 can be used for immediate process monitoring and effective disturbance detection by assessing it against reference patterns at individual L/S ratios. It is evident that a deviation affecting granule size occurred 60 s into the process, as the Dv50 during the subsequent drying period significantly diverged from the expected trend established for granules produced at the individual L/S ratio of 0.4.

The granule rate shown in Figure 13 B also reflects patterns associated with both the individual L/S ratios (0.15 and 0.4). The initial stage of filling under disturbed conditions (L/S Change), corresponds positively with the granules produced exclusively at a L/S ratio of 0.4. In both cases, a maximum granule rate of 270 granules/s (section 3.3.1.3.) is detected over the same 60 s period. Subsequent to the sudden variation to the lowest L/S ratio, the granule rate increases significantly, reaching approximately 3000 granules/s before filling concludes at 180 s, similar to granules produced under solely 0.15. As the loading phase ends and the drying process continues, the granule rate decreases considerably due to elutriation. This pattern is highly characteristic of granules produced at the low L/S ratio of 0.15 and, as observed in Figure 13 B, contrasts sharply with the behaviour at 0.4 L/S ratio, where the granule rate increases during this time.

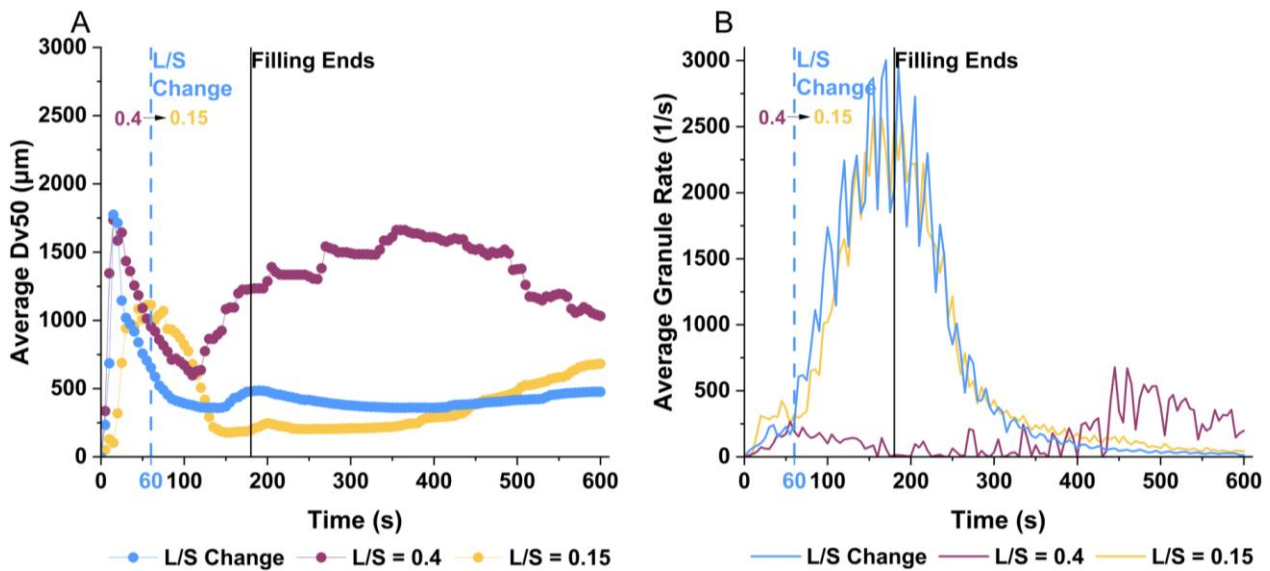


Figure 13 A comparison between the real-time averaged granules' characteristics obtained using the Parsum probe for granules produced while mimicking a manufacturing irregularity, by changing the L/S ratio during cell filling (from 0.4 to 0.15), and the individual L/S ratio ratios namely the lower (0.15) and maximum (0.4) boundaries. A: The percentile Dv50 values, B: In-line granule rate.

Figure 14 A-C displays the GSD for granules produced under normal and disturbed conditions at various processing times. An additional process time (15 s) during the filling phase is presented. At this time-point, the GSD for the lowest L/S ratio (Figure 14 A) shows a high concentration of fines (<200 µm) resulting from the significantly reduced amount of liquid binder used during granulation. In contrast, the L/S ratio disturbance presented in Figure 14 B exhibits a notable correlation with the highest L/S ratio of 0.4 (Figure 14 C), both displaying the presence of significantly larger fractions of coarse granules at the same time point (15 s), as expected.

However, as filling continues and considering the deviation produced at 60 s, the distribution in Figure 14 B exhibits an opposite behaviour as compared to the L/S ratio of 0.4. Although the filling phase defined throughout the first 180 s is mostly unstable due to the combination of processes occurring simultaneously, the disturbance becomes noticeable starting at 120 s. At this time, the GSD shows an increase fraction of fines under 200 µm (accumulated total of 25%), with only an insignificant reduction in their proportion at 180 s. This behaviour is intrinsically different from the granules produced solely at the highest L/S ratio of 0.4 (Figure 14 C) where the GSD broadens towards coarse granules. As the process reaches the established stable region (200 – 400 s) the irregularity becomes more pronounced. The GSD in Figure 14 B concentrates towards smaller granules, highly similar to the lowest L/S ratio of 0.15 (Figure 14 A). At 480 and 600 s, a slight increase in the proportion of coarse granules is detected, due to the elutriation of small granules and settling of the larger granules produced during the first 60 s.

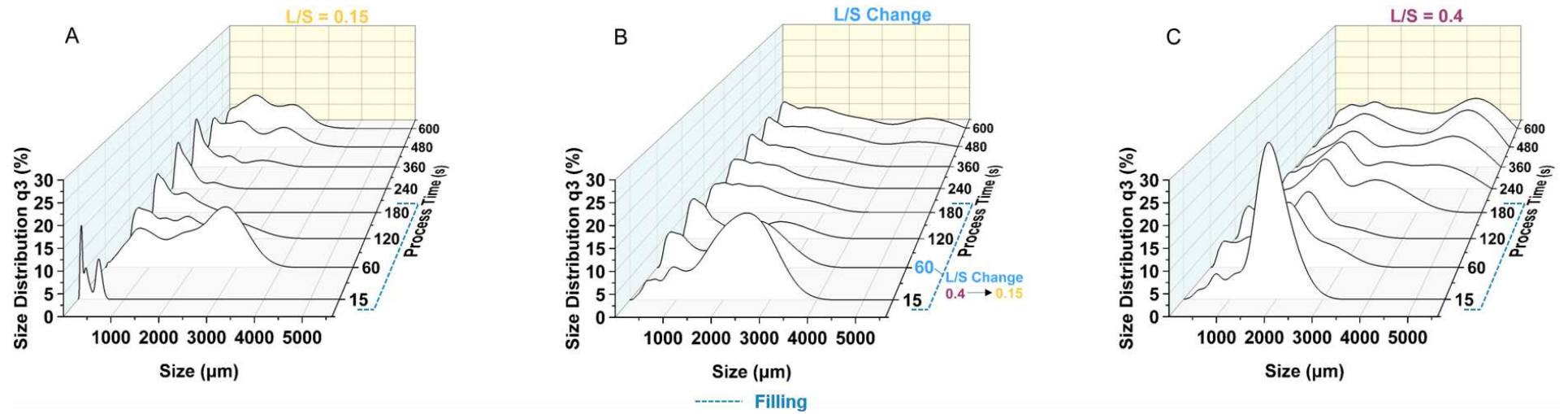


Figure 14 The in-line granule size distribution ( $q_3$ ) at various processing times throughout the fluid-bed drying process for granules produced under A: lowest L/S ratio boundary of 0.15, B: the disturbance mimicked through an in-process sudden L/S ratio variation (from 0.4 to 0.15), and C: the upper L/S ratio boundary of 0.4. Each curve represents the average of three experimental replicates at the same processing time.

## 4. CONCLUSION

This paper provides a thorough analysis of the application of in-line sensory measurement techniques within a key unit operation of the ConsiGma™25 line, facilitating a comprehensive real-time understanding of granules' size, rate and distribution throughout the segmented fluid-bed drying process. The in-line implementation of a Parsum IPP70-S probe demonstrated that the real-time measurement is not solely impacted by the individual granule passing through the optical field at a specific processing time, but is also considerably affected by granules' movement as a population during the drying process. Process related factors, including the filling phase, the activation of the blow-back system or particle segregation phenomena could significantly influence granules' behaviour throughout drying.

Granules were produced using three various L/S ratios (0.15, 0.3 and 0.4), and a real-time reference granule behaviour was established based on the volumetric percentiles ( $D_v$ ), granules' rate and the GSD. A positive relationship between the L/S ratio and granules' size was highlighted, although this correlation was observed to be more distinguishable in real-time after the filling process within the fluid-bed dryer is complete. This is due to the fact that more than one process occurs simultaneously at this stage, namely filling and drying, which promotes a chaotic granule behaviour.

Nonetheless, specific patterns related to granules' real-time measurement when utilising various L/S ratios were also highlighted. These trends were attributed to multiple factors such as granule size, moisture content, probe's operating principle and limitations or at times, to operational aspects characteristic to segmented fluid-bed drying. Granules produced at the highest L/S ratio exhibited distinctly different trends compared to those formed at lower L/S ratios. The use of a significantly higher amount of liquid binder, and the subsequent formation of a greater number of liquid bridges between particles, resulted in the formation of coarse, cohesive granules. This caused a large amount of the material to settle at the bottom of the FBD cell, further submerging the probe under the granule bed due to insufficient fluidisation. Additionally, instances of channelling during drying were reported. The rationale was validated by further analysis of real-time granules' rate, GSD and nevertheless through in-line near-infrared spectroscopy used for granule moisture content monitoring post-drying.

Measurement constraints related to the real-time granule characterisation using the Parsum probe were also examined through off-line experiments. The impact of coincidental occurrences on granule size estimation for twin-screw elongated or irregularly shaped agglomerates across various feed rates was investigated, followed by a critical analysis of the in-line FBD data. Granule overlapping instances were found to cause size overestimation, especially at high granule rates. Further investigation clarified the increased impact of such occurrences on granules'  $D_{v90}$  percentile. Additionally, it was highlighted that the possibility of multiple coarse granules passing through probe's measurement field simultaneously could cause detector saturation, potentially affecting the accurate representation of this percentile.

Lastly, to address the industrial need of real-time decision making strategies and more importantly, to align with the ICH Q13 regulatory guidelines concerning the timely identification of disturbances during production, additional measurements were carried on granules produced under a purposely created system irregularity. This was achieved through varying the L/S ratio in-process, while monitoring the probe's sensitivity to process disturbances during drying through real-time granule characterisation. The impact of the mimicked abnormality was identified in-line, information that can be further applied to detect undesired system deviations at industrial scales and nonetheless allow for real-time decision-making with the aim of reducing allocable sources of variation during CPM.

## **ACKNOWLEDGEMENTS**

The author gratefully acknowledges Prof. Agba D. Salman for his invaluable guidance throughout the development of this work, Dr. Chalak Omar and Mr. Stefan Dietrich for their technical expertise, and Mr. Simon J. Canham for his technical and experimental assistance.

## REFERENCES

- [1] W. Yang, W. Qian, Z. Yuan, B. Chen, Perspectives on the flexibility analysis for continuous pharmaceutical manufacturing processes, *Chinese Journal of Chemical Engineering* 41 (2022) 29–41.
- [2] R. Lakerveld, Chapter 16 - Control system implementation and plant-wide control of continuous pharmaceutical manufacturing pilot plant (end-to-end manufacturing process), in: R. Singh, Z. Yuan (Eds.), *Process Systems Engineering for Pharmaceutical Manufacturing: From Product Design to Enterprise-Wide Decisions*, Elsevier, Amsterdam, 2018: pp. 403–430.
- [3] D. Malevez, D. Copot, From batch to continuous tablet manufacturing: a control perspective, *IFAC-PapersOnLine* 54 (2021) 562–567.
- [4] Q. Su, S. Ganesh, M. Moreno, Y. Bommireddy, M. Gonzalez, G.V. Reklaitis, Z.K. Nagy, A perspective on Quality-by-Control (QbC) in pharmaceutical continuous manufacturing, *Computers & Chemical Engineering* 125 (2019) 216–231.
- [5] International Council for Harmonisation of Technical Requirements for Pharmaceuticals for Human Use (ICH), *ICH Guideline Q13 on Continuous Manufacturing of Drug Substances and Drug Products*, (2023).
- [6] S. Celikovic, J. Poms, J. Khinast, M. Horn, J. Rehr, Control oriented modeling of twin-screw granulation in the ConsiGmaTM-25 production plant, *International Journal of Pharmaceutics* 641 (2023) 123038.
- [7] D. Monaco, C. Omar, G.K. Reynolds, P. Tajarobi, J.D. Litster, A.D. Salman, Drying in a continuous wet granulation line: Investigation of different end of drying control methods, *Powder Technology* 392 (2021) 157–166.
- [8] E.-A. Jung, Y.-J. Park, J.-E. Kim, Application of continuous manufacturing for solid oral dosage forms, *J. Pharm. Investig.* 53 (2023) 457–474.
- [9] V. Pauli, Y. Roggo, P. Kleinebudde, M. Krumme, Real-time monitoring of particle size distribution in a continuous granulation and drying process by near infrared spectroscopy, *European Journal of Pharmaceutics and Biopharmaceutics* 141 (2019) 90–99.
- [10] R.M. Dhenge, R.S. Fyles, J.J. Cartwright, D.G. Doughty, M.J. Hounslow, A.D. Salman, Twin screw wet granulation: Granule properties, *Chemical Engineering Journal* 164 (2010) 322–329.
- [11] E.J. Kim, J.H. Kim, M.-S. Kim, S.H. Jeong, D.H. Choi, Process Analytical Technology Tools for Monitoring Pharmaceutical Unit Operations: A Control Strategy for Continuous Process Verification, *Pharmaceutics* 13 (2021) 919.
- [12] A. Junnila, H. Wikström, A. Megarry, A. Gholami, F. Papathanasiou, A. Blomberg, J. Ketolainen, P. Tajarobi, Faster to First-time-in-Human: Prediction of the liquid solid ratio for continuous wet granulation, *European Journal of Pharmaceutical Sciences* 172 (2022) 106151.
- [13] C. Portier, K. Pandelaere, U. Delaet, T. Vigh, A. Kumar, G. Di Pretoro, T. De Beer, C. Vervaet, V. Vanhoorne, Continuous twin screw granulation: Influence of process and formulation variables on granule quality attributes of model formulations, *International Journal of Pharmaceutics* 576 (2020) 118981.
- [14] R.M. Dhenge, J.J. Cartwright, M.J. Hounslow, A.D. Salman, Twin screw wet granulation: Effects of properties of granulation liquid, *Powder Technology* 229 (2012) 126–136.
- [15] M. Verstraeten, D. Van Hauwermeiren, K. Lee, N. Turnbull, D. Wilsdon, M. am Ende, P. Doshi, C. Vervaet, D. Brouckaert, S.T.F.C. Mortier, I. Nopens, T.D. Beer, In-depth experimental analysis of pharmaceutical twin-screw wet granulation in view of detailed process understanding, *International Journal of Pharmaceutics* 529 (2017) 678–693.

- [16] A.S. El Hagrasy, J.R. Hennenkamp, M.D. Burke, J.J. Cartwright, J.D. Litster, Twin screw wet granulation: Influence of formulation parameters on granule properties and growth behavior, *Powder Technology* 238 (2013) 108–115.
- [17] A. Kumar, J. Dhondt, J. Vercruyssen, F. De Leersnyder, V. Vanhoorne, C. Vervaet, J.P. Remon, K.V. Gernaey, T. De Beer, I. Nopens, Development of a process map: A step towards a regime map for steady-state high shear wet twin screw granulation, *Powder Technology* 300 (2016) 73–82.
- [18] S.F. Islam, S.M. Hawkins, J.L.L. Meyer, A.R.C. Sharman, Evaluation of different particle size distribution and morphology characterization techniques, *Additive Manufacturing Letters* 3 (2022) 100077.
- [19] A.F.T. Silva, A. Burggraef, Q. Denon, P. Van der Meeren, N. Sandler, T. Van Den Kerkhof, M. Hellings, C. Vervaet, J.P. Remon, J.A. Lopes, T. De Beer, Particle sizing measurements in pharmaceutical applications: Comparison of in-process methods versus off-line methods, *European Journal of Pharmaceutics and Biopharmaceutics* 85 (2013) 1006–1018.
- [20] D. Petrak, S. Dietrich, E. Günter, K. Michael, In-line particle sizing for real-time process control by fibre-optical spatial filtering technique (SFT), *Advanced Powder Technology* 22 (2011) 203–208.
- [21] K. Roßteuscher-Carl, S. Fricke, M.C. Hacker, M. Schulz-Siegmund, In-line monitoring of particle size in a fluid bed granulator: Investigations concerning positioning and configuration of the sensor, *International Journal of Pharmaceutics* 466 (2014) 31–37.
- [22] M. Langner, I. Kitzmann, A.-L. Ruppert, I. Wittich, B. Wolf, In-line particle size measurement and process influences on rotary fluidized bed agglomeration, *Powder Technology* 364 (2020) 673–679.
- [23] R.F. Nascimento, M.F. Ávila, O.P. Taranto, L.E. Kurozawa, A new approach to the mechanisms of agglomeration in fluidized beds based on Spatial Filter Velocimetry measurements, *Powder Technology* 393 (2021) 219–228.
- [24] F. Foltmann, K. Knop, P. Kleinebudde, M. Pein, In-line spatial filtering velocimetry for particle size and film thickness determination in fluidized-bed pellet coating processes, *European Journal of Pharmaceutics and Biopharmaceutics* 88 (2014) 931–938.
- [25] G. Hudovornik, K. Korasa, F. Vrečer, A study on the applicability of in-line measurements in the monitoring of the pellet coating process, *European Journal of Pharmaceutical Sciences* 75 (2015) 160–168.
- [26] A. Dular Vovko, B. Hodžić, G. Hudovornik, F. Vrečer, Implementation of spatial filtering technique in monitoring roller compaction process, *International Journal of Pharmaceutics* 606 (2021) 120896.
- [27] A. Dular Vovko, T. Slak, Z. Simončič, F. Vrečer, G. Hudovornik, The influence of milling of ribbons on selected granule quality attributes and carvedilol release from roller-compacted hypromellose-based matrix tablets, *Journal of Drug Delivery Science and Technology* 98 (2024) 105882.
- [28] L. Madarász, Á. Köte, B. Hambalkó, K. Csorba, V. Kovács, L. Lengyel, G. Marosi, A. Farkas, Z.K. Nagy, A. Domokos, In-line particle size measurement based on image analysis in a fully continuous granule manufacturing line for rapid process understanding and development, *International Journal of Pharmaceutics* 612 (2022) 1–8.
- [29] S. Celikovic, J. Poms, J. Khinast, M. Horn, J. Rehr, Development and Application of Control Concepts for Twin-Screw Wet Granulation in the ConsiGma™-25: Part 2 Granule Size, *International Journal of Pharmaceutics* 657 (2024) 124125.
- [30] M. Fonteyne, J. Vercruyssen, D.C. Díaz, D. Gildemyn, C. Vervaet, J.P. Remon, T.D. Beer, Real-time assessment of critical quality attributes of a continuous granulation process, *Pharmaceutical Development and Technology* 18 (2013) 85–97.

- [31] A. Burggraefe, T. Van Den Kerkhof, M. Hellings, J.P. Remon, C. Vervaet, T. De Beer, Evaluation of in-line spatial filter velocimetry as PAT monitoring tool for particle growth during fluid bed granulation, *European Journal of Pharmaceutics and Biopharmaceutics* 76 (2010) 138–146.
- [32] G.D. Tovey, ed., *Pharmaceutical Formulation: The Science and Technology of Dosage Forms*, Royal Society of Chemistry, Cambridge, UK, 2018.
- [33] C. Portier, K. Pandelaere, U. Delaet, T. Vigh, G. Di Pretoro, T. De Beer, C. Vervaet, V. Vanhoorne, Continuous twin screw granulation: A complex interplay between formulation properties, process settings and screw design, *International Journal of Pharmaceutics* 576 (2020) 119004.
- [34] V. Vanhoorne, B. Vanbillemont, J. Vercruyssen, F. De Leersnyder, P. Gomes, T.D. Beer, J.P. Remon, C. Vervaet, Development of a controlled release formulation by continuous twin screw granulation: Influence of process and formulation parameters, *International Journal of Pharmaceutics* 505 (2016) 61–68.
- [35] K. Matsunami, A. Ryckaert, M. Peeters, S. Badr, H. Sugiyama, I. Nopens, T. De Beer, Analysis of the Effects of Process Parameters on Start-Up Operation in Continuous Wet Granulation, *Processes* 9 (2021) 1502.
- [36] Q. Zou, X. Jia, T. Zhang, J. Liang, Effects of water-based SiO<sub>2</sub> nanofluids on the wettability of coal dust and particle deposition characteristics, *Advanced Powder Technology* 35 (2024) 104308.
- [37] N. Maclean, I. Khadra, J. Mann, H. Williams, A. Abbott, H. Mead, D. Markl, Investigating the role of excipients on the physical stability of directly compressed tablets, *Int J Pharm X* 4 (2021) 100106.
- [38] B. Yang, Wei, Chen, Yang, Yang, Wang, Qifang, S. and Li, Evaluation about wettability, water absorption or swelling of excipients through various methods and the correlation between these parameters and tablet disintegration, *Drug Development and Industrial Pharmacy* 44 (2018) 1417–1425.
- [39] S.Y. Misyura, V.S. Morozov, V.A. Andryushchenko, E.G. Orlova, Effect of temperature and capillary number on wettability and contact angle hysteresis of various materials. Modeling taking into account porosity, *Materials Science and Engineering: B* 311 (2025) 117827.
- [40] G. Buckton, Assessment of the wettability of pharmaceutical powders, *Journal of Adhesion Science and Technology* 7 (1993) 205–219.
- [41] X. Dai, J. Wang, B. Yan, Q. Wang, Y. Shen, Y. Chen, Y. Tian, A Novel Lactose/MCC/L-HPC Triple-Based Co-Processed Excipients with Improved Tableting Performance Designed for Metoclopramide Orally Disintegrating Tablets, *Pharmaceutics* 16 (2024) 959.
- [42] P. Diós, T. Pernecker, S. Nagy, S. Pál, A. Dévay, Influence of different types of low substituted hydroxypropyl cellulose on tableting, disintegration, and floating behaviour of floating drug delivery systems, *Saudi Pharm J* 23 (2015) 658–666.
- [43] E.P. Cox, A Method of Assigning Numerical and Percentage Values to the Degree of Roundness of Sand Grains, *Journal of Paleontology* 1 (1927) 179–183.
- [44] S. Dražić, N. Sladoje, J. Lindblad, Estimation of Feret's diameter from pixel coverage representation of a shape, *Pattern Recognition Letters* 80 (2016) 37–45.
- [45] M.J. Rhodes, *Introduction to particle technology*, 2nd ed, Wiley, Chichester, England ; Hoboken, NJ, 2008.